Article

NK2R control of energy expenditure and feeding to treat metabolic diseases

Frederike Sass[1,2,19], Tao Ma[1,19], Jeppe H. Ekberg[1,3], Melissa Kirigiti[4], Mario G. Ureña[1], Lucile Dollet[1], Jenny M. Brown[1,5], Astrid L. Basse[1], Warren T. Yacawych[6,7], Hayley B. Burm[1], Mette K. Andersen[1], Thomas S. Nielsen[1], Abigail J. Tomlinson[6], Oksana Dmytiyeva[1], Dan P. Christensen[1,3], Lindsay Bader[4], Camilla T. Vo[1,8], Yaxu Wang[2,9], Dylan M. Rausch[1], Cecilie K. Kristensen[1], María Gestal-Mato[1], Wietse In het Panhuis[10], Kim A. Sjøberg[1], Stace Kernodle[11], Jacob E. Petersen[1], Artem Pavlovskyi[1], Manbir Sandhu[2,9], Ida Moltke[12], Marit E. Jørgensen[13,14,15], Anders Albrechtsen[12], Niels Grarup[1], M. Madan Babu[2,9], Patrick C. N. Rensen[10], Sander Kooijman[10], Randy J. Seeley[11], Anna Worthmann[16], Joerg Heeren[16], Tune H. Pers[1,5], Torben Hansen[1], Magnus B. F. Gustafsson[3,17], Mads Tang-Christensen[3,18], Tuomas O. Kilpeläinen[1,5], Martin G. Myers Jr[6,7], Paul Kievit[4], Thue W. Schwartz[1,3], Jakob B. Hansen[1,3 ✉] & Zachary Gerhart-Hines[1,2,3 ✉]

The combination of decreasing food intake and increasing energy expenditure represents a powerful strategy for counteracting cardiometabolic diseases such as obesity and type 2 diabetes[1]. Yet current pharmacological approaches require conjugation of multiple receptor agonists to achieve both effects[2–4], and so far, no safe energy-expending option has reached the clinic. Here we show that activation of neurokinin 2 receptor (NK2R) is sufficient to suppress appetite centrally and increase energy expenditure peripherally. We focused on NK2R after revealing its genetic links to obesity and glucose control. However, therapeutically exploiting NK2R signalling has previously been unattainable because its endogenous ligand, neurokinin A, is short-lived and lacks receptor specificity[5,6]. Therefore, we developed selective, long-acting NK2R agonists with potential for once-weekly administration in humans. In mice, these agonists elicit weight loss by inducing energy expenditure and non-aversive appetite suppression that circumvents canonical leptin signalling. Additionally, a hyperinsulinaemic–euglycaemic clamp reveals that NK2R agonism acutely enhances insulin sensitization. In diabetic, obese macaques, NK2R activation significantly decreases body weight, blood glucose, triglycerides and cholesterol, and ameliorates insulin resistance. These findings identify a single receptor target that leverages both energy-expending and appetite-suppressing programmes to improve energy homeostasis and reverse cardiometabolic dysfunction across species.

The development of long-acting pharmacotherapies based on the incretin hormones—glucagon-like peptide-1 (GLP-1), glucose-dependent insulinotropic peptide (GIP) and glucagon (GCG)—has been transformative for the treatment of cardiometabolic diseases such as obesity and type 2 diabetes (T2D)[2,7–11]. GLP-1 receptor agonists and GLP-1R/GIPR dual agonists are able to help an appreciable number of individuals living with obesity to achieve sustained weight loss similar to the levels obtained through the current 'gold standard', bariatric surgery[12–14]. Yet for people living with both obesity and T2D, a group of more than 380 million people globally, the weight-lowering efficacy of GLP-1-derived pharmacotherapies is significantly reduced compared with those individuals with obesity but without T2D[10,12,15]. The mechanistic underpinnings of this blunted weight-lowering efficacy of GLP-1 receptor agonists remain unknown but represent a major unmet need for the population with T2D. Additionally, although the current approved options and next generation of treatments (for example,

[1]Novo Nordisk Foundation Center for Basic Metabolic Research, University of Copenhagen, Copenhagen, Denmark. [2]Center for Adipocyte Signaling (ADIPOSIGN), University of Southern Denmark, Odense, Denmark. [3]Embark Laboratories, Copenhagen, Denmark. [4]Division of Metabolic Health and Disease, Oregon National Primate Research Center, Oregon Health & Science University, Portland, OR, USA. [5]The Novo Nordisk Foundation Center for Genomic Mechanisms of Disease, Broad Institute of MIT and Harvard, Cambridge, MA, USA. [6]Department of Internal Medicine, University of Michigan, Ann Arbor, MI, USA. [7]Department of Molecular and Integrative Physiology, University of Michigan, Ann Arbor, MI, USA. [8]Neuroscience Academy Denmark, Copenhagen, Denmark. [9]Center of Excellence for Data Driven Discovery, Department of Structural Biology, St Jude Children's Research Hospital, Memphis, TN, USA. [10]Department of Medicine, Division of Endocrinology and Einthoven Laboratory of Experimental Vascular Medicine, Leiden University Medical Center, Leiden, the Netherlands. [11]Department of Surgery, University of Michigan, Ann Arbor, MI, USA. [12]Section for Computational and RNA Biology, Department of Biology, University of Copenhagen, Copenhagen, Denmark. [13]Clinical Research, Copenhagen University Hospital - Steno Diabetes Center Copenhagen, Herlev, Denmark. [14]Centre for Public Health in Greenland, National Institute of Public Health, University of Southern Denmark, Copenhagen, Denmark. [15]Steno Diabetes Center Greenland, Nuuk, Greenland. [16]Department of Biochemistry and Molecular Cell Biology, University Medical Center Hamburg-Eppendorf, Hamburg, Germany. [17]Chemical Process Research and Development, Chemical Process Research & DevelopmentLEO Pharma, Ballerup, Denmark. [18]School of Biomedical Sciences Faculty of Medicine, Nursing and Health Sciences Monash University, Melbourne, Victoria, Australia. [19]These authors contributed equally: Frederike Sass, Tao Ma. ✉e-mail: jbh@embarklaboratories.com; zpg@sund.ku.dk

Article

amylin receptor agonists[16]) have made major strides in producing lasting and more tolerable appetite suppression, a key gap is the lack of a means to increase energy expenditure. The importance of targeting energy expenditure is particularly relevant given the steady decline in basal metabolic rate in the population over the past 40 years[17].

In the 1930s, the mitochondrial uncoupler dinitrophenol demonstrated the powerful therapeutic potential of energy dissipation on weight loss[18]. However, dinitrophenol and more recent attempts to leverage energy expenditure, such as peripheral beta-adrenergic activation, have been burdened with narrow safety windows, cardiovascular concerns and translational hurdles across species[1]. Most recently, glucagon receptor (GCGR) agonism has proved to be an especially promising candidate for boosting catabolic metabolism[3,4,19], although increases in heart rate and hepatic glucose production and questions surrounding loss of lean mass[20,21] could potentially limit its applicability, particularly in the context of T2D. However, polypharmaceutical approaches that conjugate GCGR agonists to insulinotropic drivers such as GLP-1, with or without GIP (that is, triple or dual agonists, respectively) may help mitigate these undesirable effects and enable GCGR agonism to meaningfully contribute to treating cardiometabolic indications[22].

From a T2D standpoint, despite insulin-sensitizing thiazolidinediones, GLP-1-based therapies and the sodium–glucose cotransporter 2 inhibitor (sGLT2i) class of glucose-lowering agents, some patients still progress to a regimen of increasing insulin doses to combat insulin resistance, which is likely to serve to further exacerbate weight gain. To this end, new mechanisms of glucose and lipid clearance have become attractive targets. Nevertheless, the landmark clinical breakthroughs ushered in by the incretin family solidly underscore the unprecedented therapeutic potential of G-protein-coupled receptors (GPCRs) across cardiometabolic indications. GPCRs are already the most druggable proteins throughout pharmacology owing, in large part, to their cell-type selectivity and surface accessibility[23]. Therefore, we initially set out to identify other GPCRs that might address remaining critical unmet needs for people living with both obesity and T2D. We identified a conserved GPCR pathway capable of not only peripherally promoting energy expenditure and insulin sensitization but also centrally reducing appetite.

Genetics of NK2R and metabolic health

To first enrich for candidate receptors that might be especially effective in a diabetic context, we leveraged the publicly available database, HugeAMP Type 2 Diabetes Knowledge Portal (T2D-KP)[24], which contains human genetic associations assembled from over 350 studies. We compiled and ranked the loci of more than 380 non-odorant GPCRs according to their significance of association with haemoglobin A1c (HbA1c) levels, a primary clinical indicator of glucose control and diabetes progression[25]. We found that the most significant association was with the region containing the neurokinin 2 receptor (NK2R) gene (also known as tachykinin receptor 2 (TACR2)) (Fig. 1a). NK2R is a G_q-coupled receptor that is classically studied for its role in the gastrointestinal tract and the central nervous system[5] (CNS) but—to our knowledge—has not previously been linked to glucose homeostasis or cardiometabolic health. However, the presence of two closely adjacent genes, tetraspanin 15 (TSPAN15) and hexokinase 1 (HK1), complicates the investigation of HbA1c and other trait associations to NK2R variants, particularly since HK1 is already significantly linked to HbA1c levels through effects on erythrocyte metabolism and turnover[26,27].

Given this strong link between HbA1c and HK1, we initially focused on coding variants in NK2R from an exome sequencing dataset[28]. Functional investigation revealed that four missense variants, I23T (rs5030920; minor allele frequency (MAF) = 23.6%), R323H (rs61732393; MAF = 0.10%), V54I (rs151093941; MAF = 0.025%) and A161T (rs148031991; MAF = 0.102%), reduced NK2R signalling capacity of which two, I23T and R323H, were further associated with increased HbA1c levels in the UK Biobank (Fig. 1b and Extended Data Fig. 1a). We additionally found modest associations between these variants and fasting glucose, cholesterol, fat distribution, liver enzymes and total bilirubin (Extended Data Table 1). However, gene-based association tests for HbA1c, which were dominated by HK1 (Extended Data Table 2), suggested that missense variants alone would not provide a meaningful resolution of the specific effects attributable to NK2R.

Therefore, to more comprehensively investigate NK2R genetic contributions, we assessed summary statistics on HbA1c associations in the greater NK2R-containing locus (including the adjacent genes hexokinase domain-containing 1 (HKDC1), HK1 and TSPAN15) from a European-ancestry meta-analysis comprising 438,069 individuals[29]. In this region, we identified 978 variants with genome-wide significant associations for HbA1c ($P < 5 \times 10^{-8}$) of which 16 were independent lead variants[30] ($r^2 < 0.01$ within ±1 Mb) (Table 1). Fine mapping of HbA1c associations using CARMA[31] revealed 9 candidate causal variants with a posterior inclusion probability of less than 0.1 (Table 2). These variants represent four distinct signals within HKDC1 (three variants), HK1 (four variants), NK2R (one variant) and TSPAN15 (one variant) (Extended Data Fig. 1b). The NK2R variant rs791147 (MAF = 26.2–48.4%) is intronic and significantly associated with NK2R expression in several tissues, including the brain, adipose tissue, macrophages and skeletal muscle (Table 3), suggesting that it may regulate NK2R expression and HbA1c levels. For a better resolution of tissue-specific expression regulation and HbA1c associations, we performed gene-based transcriptome-wide association studies (TWASs) using PrediXcan. We found that increased NK2R expression in the nucleus accumbens (ACB) of the brain was associated with decreased HbA1c levels, with or without adjustment for body mass index (BMI), whereas expression of HK1 and TSPAN15 were not (Fig. 1c and Table 4).

We next complemented the large-scale analyses of Western Europeans with an assessment of NK2R variant associations in the more isolated Greenlandic population, which has a unique genetic architecture due to its geographical location and population history. The Greenlandic population has similar rates of cardiometabolic disease as Europeans and has previously revealed valuable genetic insights that are masked or absent in larger European cohorts[32]. Associations with traits related to glucose homeostasis were not found in the Greenlandic cohort; however, there were modest associations with obesity-related phenotypes (Extended Data Table 3). Specifically, the strongest associations were observed for the non-coding variant rs139900276 in the 5′ untranslated region of NK2R. This variant was significantly associated with reduced BMI, body weight, waist–hip ratio, waist–height ratio and fat percentage (Fig. 1d). Furthermore, carriers of rs139900276 in the Greenlandic population had significantly higher expression of NK2R (by transcriptional profiling of whole blood) (Fig. 1e), suggesting that NK2R expression was inversely related to obesity parameters. Collectively, the glycaemic and obesity genetic associations from different populations suggest that NK2R signalling may have a role in energy homeostasis in humans, and therefore represents an interesting target for metabolic investigation.

To evaluate the effect of pharmacological activation of NK2R signalling on mammalian metabolic homeostasis in vivo, the endogenous NK2R ligand, neurokinin A (NKA), was administered subcutaneously to diet-induced obese (DIO) mice. Mice were dosed twice daily, given that native NKA has a markedly short half-life of minutes (Fig. 1f). This regimen of NKA administration (Fig. 1g) was well tolerated and acutely increased oxygen consumption (Fig. 1h). During 9 days of repeated injections in DIO mice, food intake (Fig. 1i), body weight (Fig. 1j) and inguinal (iWAT) and epididymal (eWAT) white adipose tissue (Fig. 1k) were reduced in NKA-treated mice and insulin tolerance was improved relative to vehicle controls (Fig. 1l). Yet despite the beneficial effects of NK2R agonism, the rapid clearance of NKA precluded an accurate assessment of the bona fide therapeutic potential of NK2R. Therefore, we generated a longer-acting peptide (hereby referred to as EB0014)
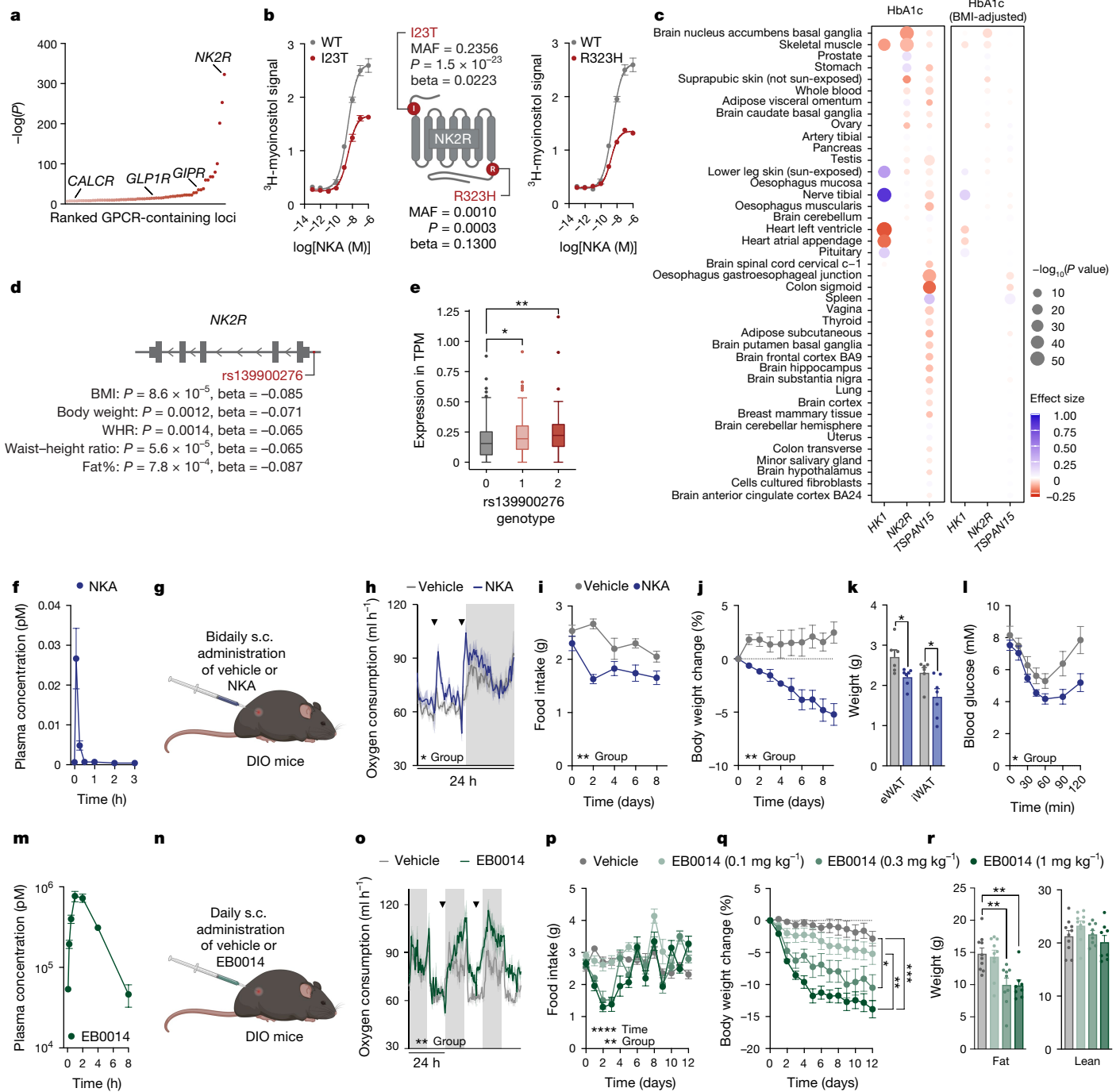
Fig. 1 | NK2R agonism is genetically and functionally linked to cardiometabolic protection. a, Ranked P values for HbA1c associations of 381 non-odorant GPCR loci (±50 kb) from T2D-KP. **b**, Gq signalling and HbA1c associations of the *NK2R* missense variants I23T and R323H ($n = 2$ per variant). **c**, TWAS of *HK1*, *NK2R* and *TSPAN15* and HbA1c levels, with and without adjustment for BMI. **d**,**e**, Obesity-related anthropometric associations of the *NK2R* non-coding variant rs139900276 in the Greenlandic cohort (**d**) and *NK2R* expression stratified by rs139900276 genotype (**e**). WHR, waist–hip ratio. **f**, Pharmacokinetics of NKA ($n = 3$ mice). **g**–**k**, In vivo effects of a twice daily subcutaneous (s.c.) injection of vehicle or 1 mg kg^{-1} NKA (**g**) on oxygen consumption ($n = 6$ mice per group) (**h**), food intake (**i**) and body weight (**j**)

and white adipose tissue weight (**k**) at study conclusion ($n = 6$ (vehicle), $n = 7$ mice (NKA)). **l**, Insulin tolerance test of DIO mice treated with vehicle ($n = 6$) or NKA ($n = 7$) twice daily for 12 days. **m**, Pharmacokinetics of EB0014 ($n = 3$ mice). **n**,**o**, In vivo effects of daily subcutaneous injections of vehicle or 1 mg kg^{-1} EB0014 (**n**) on oxygen consumption (**o**; $n = 6$ mice per group). **p**–**r**, Dose-dependent changes in food intake (**p**), weight loss (**q**) and body composition (**r**) after 12 days of daily injections ($n = 10$ (vehicle, 0.1 mg kg^{-1}), $n = 9$ (0.3 mg kg^{-1}), $n = 8$ mice (1 mg kg^{-1})). Arrowheads indicate time of injection of vehicle or agonist (**h**,**o**). Data are mean ± s.e.m. (**b**,**f**,**h**–**m**,**o**–**r**); box plots present median and Tukey's whiskers (**e**). *$P < 0.05$, **$P < 0.01$, ***$P < 0.005$, ****$P < 0.0001$. Detailed statistics are in the Supplementary Information and Source Data.

in which a 16-carbon fatty acid, called C16-gammaGlu (C16GG, the side chain used in the GLP-1R agonist liraglutide[33]), was covalently attached to Lys2 of native NKA to increase retention in the blood from minutes to hours, probably via albumin binding (Fig. 1m). Daily

injections of EB0014 (Fig. 1n) robustly induced oxygen consumption (Fig. 1o), decreased food intake during the initial days of treatment (Fig. 1p) and dose-dependently reduced body weight (Fig. 1q), which was driven by loss of fat mass (Fig. 1r). Transient loose stools were

Table 1 | Results for linkage disequilibrium (LD) clumping in the *HKDC1–HK1–NK2R–TSPAN15* region (10:70929740–71367422)

Variant	Base-pair location	A1	AO	AFR MAF	AMR MAF	EAS MAF	EUR MAF	SAS MAF	Beta	s.e.	*P*	Closest gene (consequence)
rs143849423	10:70969723	G	T	0.0008	0.0140	0.0000	0.0159	0.0050	0.0363	0.0064	1.74×10^{-8}	*HKDC1* (downstream gene variant)
rs72814215	10:70998703	G	A	0.0008	0.0060	0.0000	0.0139	0.0070	0.0580	0.0090	1.21×10^{-10}	*HKDC1* (intron variant)
10:71002040	10:71002040	T	TG	NA	NA	NA	0.4105	NA	0.0653	0.0019	7.52×10^{-257}	*HKDC1* (intron variant)
10:71069872	10:71069872	T	TA	NA	NA	NA	0.1777	NA	0.0204	0.0027	8.62×10^{-14}	*HK1* (NA)
rs5030918	10:71078526	A	C	0.000	0.0010	0.0000	0.0149	0.0020	0.2872	0.0063	0	*HK1* (intron variant)
rs2015803	10:71081399	T	C	0.4675	0.4860	0.2480	0.2664	0.2700	0.0455	0.0021	6.32×10^{-101}	*HK1* (intron variant)
10:71118821	10:71118821	AAG	A	NA	NA	NA	0.0401	NA	0.3077	0.0049	0	*HK1* (NA)
rs9299503	10:71136050	A	G	0.3109	0.4510	0.1935	0.4930	0.1935	0.0533	0.0020	1.87×10^{-157}	*HK1* (intron variant)
rs4745984	10:71143488	C	A	0.0144	0.3520	0.3254	0.0984	0.0700	0.0472	0.0031	1.79×10^{-53}	*HK1* (intron variant)
10:71144995	10:71144995	C	CTT	NA	NA	NA	0.0635	NA	0.0418	0.0039	1.20×10^{-26}	*HK1* (NA)
rs117056999	10:71154564	T	C	0.0030	0.0100	0.0000	0.0288	0.0030	0.0400	0.0054	1.22×10^{-13}	*HK1* (intron variant)
rs1236903	10:71198994	C	G	0.0030	0.0320	0.0000	0.0795	0.0150	0.0269	0.0040	1.77×10^{-11}	*TSPAN15* (intergenic)
rs77356330	10:71205544	C	T	0.0030	0.0320	0.000	0.0378	0.0060	0.0308	0.0042	2.48×10^{-13}	*TSPAN15* (regulatory region variant)
rs72811732	10:71227549	A	T	0.0008	0.0190	0.0000	0.0368	0.0030	0.0444	0.0053	7.96×10^{-17}	*TSPAN15* (intron variant)
rs11598811	10:71288098	A	G	0.0023	0.0760	0.0000	0.0716	0.0150	0.0307	0.0037	1.46×10^{-16}	*NEUROG3* (upstream gene variant)

Results for the 16 independent variants ($r^2 < 0.01$ in 1,000 kb) in the region with minor allele frequencies from 5 genetic ancestries: African (AFR), admixed American (AMR), East Asian (EAS), European (EUR) and South Asian (SAS). The variant ID is from dbSNP, the base-pair locations are in build 37 and the annotations are from Variant Effect Predictor. The association tests were two-sided without multiple corrections. A1, effect allele; AO, other allele; s.e., standard error; NA, variant not found in the reference panel.

initially noted in the mice at the highest dose but the compound was otherwise well tolerated. These functional data uncover a paradigm of homeostatic control whereby NK2R agonism is capable of simultaneously inducing energy expenditure and decreasing food intake. The genetic variants provide further support that this signalling pathway affects HbA1c in humans and pharmacological activation of NK2R might be a new route through which to counteract cardiometabolic diseases.

Development of long-acting NK2R agonists

Although NKA and long-acting EB0014 mediated several beneficial cardiometabolic effects, it remained unknown whether these effects were mediated by NKR2. NKA is a naturally unselective peptide within the tachykinin family, and signals through both NK1R and NK3R with nearly equal potency to its cognate receptor, NK2R[6] (Fig. 2a). This lack of selectivity is a particular liability with respect to NK1R signalling, which

Table 2 | HbA1c associations of the nine genome-wide significant and causal variants in the overlapping the *HKDC1–HK1–NK2R–TSPAN15* region (10:70929740–71367422)

Variant	Base-pair location	A1	AO	AFR MAF	AMR MAF	EAS MAF	EUR MAF	SAS MAF	Beta	s.e.	*P*	Consequence	PIP	Lead (r^2)
rs72814215	10:70998703	G	A	0.0008	0.0060	0.0000	0.0139	0.0070	0.0580	0.0090	1.21×10^{-10}	*HKDC1* intron	1.0000	rs72814215 ($r^2 = 1.00$)
rs112258245	10:71001310	A	G	0.0219	0.1100	0.0000	0.1670	0.0450	0.0334	0.0026	5.92×10^{-37}	*HKDC1* intron	0.6636	rs5785903 ($r^2 = 0.26$)
rs72814226	10:71001449	G	C	0.0219	0.110	0.0000	0.1670	0.0450	0.0333	0.0026	7.91×10^{-37}	*HKDC1* intron	0.3364	rs5785903 ($r^2 = 0.26$)
rs10823338	10:71065977	G	T	0.4145	0.5060	0.2649	0.2515	0.2700	0.0386	0.0022	1.03×10^{-67}	*HK1* intron	1.0000	rs2015803 ($r^2 = 0.79$)
rs16926246	10:71093392	C	T	0.1747	0.0810	0.0010	0.1412	0.0540	0.2642	0.0027	0	*HK1* intron	1.0000	rs5030918 ($r^2 = 0.07$)
rs17476364	10:71094504	T	C	0.0015	0.0610	0.0010	0.0994	0.0170	0.3189	0.0030	0	*HK1* intron	1.0000	rs5030918 ($r^2 = 0.10$)
rs6480402	10:71095378	A	C	0.3767	0.2590	0.1319	0.2942	0.4350	0.1301	0.0021	0	*HK1* intron	1.0000	rs5030918 ($r^2 = 0.02$)
rs7911347	10:71170287	A	C	0.2912	0.4310	0.2619	0.4841	0.3190	0.0105	0.0019	2.99×10^{-8}	*NK2R* intron	0.9965	rs200572185 ($r^2 = 0.02$)
rs142394825	10:71236395	G	C	0	0.0100	0	0.0119	0.0010	0.0888	0.0083	1.25×10^{-26}	*TSPAN15* intron	1.0000	rs4745984 ($r^2 = 0.09$)

Results for the associations of 9 candidate causal (posterior inclusion probability (PIP) > 0.1) HbA1c variants in the 10:70929740–71367422 region. Fine mapping was computed with CARMA software utilizing HbA1c European summary statistics from ref. 29. All variants are located in introns, three in *HKDC1*, four in *HK1*, one in *NK2R* and one in *TSPAN15*. Additionally, the minor allele frequencies for five different genetic ancestries were added: African, admixed American, East Asian, European and South Asian. Finally, for each candidate causal variant the lead variant with the highest correlation measured in r^2 was added. The variant ID is from dbSNP, the base-pair locations are in build 37 and the annotations from Variant Effect Predictor. The association tests were two-sided without multiple corrections.

Table 3 | eQTL associations for r7911347-A available in Open Target Genetics

rs7911347-A	Adipose (Fusion)	Adipose (TwinsUK)	Brain DLPFC (ROSEMAP)	Muscle (FUSION)	Macrophage (ref. 61)	Monocyte influenza 6 h (ref. 62)
HK1	NA	NA	NA	NA	NA	NA
NK2R	0.397, $P=3.2\times10^{-33}$	0.370, $P=1.2\times10^{-19}$	0.165, $P=2.7\times10^{-10}$	1.11, $P=4.0\times10^{-63}$	0.294, $P=8.3\times10^{-13}$	NA
TSPAN15	NA	NA	0.106, $P=3.5\times10^{-5}$	NA	NA	0.549, $P=1.9\times10^{-13}$

Results are included for the tissues with reported expression quantitative trait loci (eQTL) associations for *HK1*, *NK2R* and *TSPAN15*. No eQTL associations were found for *HK1*. The association tests were two-sided without multiple corrections. NA, not applicable.

is linked to CNS disorders, inflammation, cardiopulmonary disruption, bronchoconstriction and nociception (pain sensing)[5]. Thus, despite the encouraging efficacy of the protracted NKA molecule, EB0014, NK2R selectivity is necessary to pharmacologically leverage this signalling pathway for therapeutic gain. As a starting point for developing highly NK2R-specific long-acting agonists, we took advantage of a previously described truncated NKA analogue, neurokinin A (4–10)-S5K/L9mL/M10Nle (where mL is methylleucine and Nle is norleucine), which has been shown to exhibit some degree of selectivity[34].

A single replacement of Phe at position 6 with a structurally similar Tyr conferred complete NK2R selectivity and generated the analogue neurokinin A (4–10)-S5K/F6Y/L9mL/M10Nle (called EB1001 here) (Fig. 2b). In the EB1000 compound series, we also changed the protraction strategy, substituting C16GG with a 2×(8-amino-3,6-dioxaoctanoic acid)-γGlu-C18-diacid moiety (C18DOGG; the side chain used in the GLP-1R agonist semaglutide) owing to its superior albumin affinity and water solubility compared with C16GG. We further optimized EB1001 by replacing the Nle at position 10 with a methoxinine (Mox) residue, to preserve hydrogen-bonding capacity, in an analogue, neurokinin A (4–10)-S5K/F6Y/L9mL/M10Mox (called EB1002 here) (Fig. 2b). Like EB1001, EB1002 is highly selective against NK1R on both mouse tachykinin receptors (Extended Data Fig. 2a,b) and human tachykinin receptors (Fig. 2c and Extended Data Fig. 2c) and has a markedly longer half-life in mice (10.3 h for EB1002 compared with 5.5 h for EB1001) (Fig. 2d).

To assess the mode of action of NK2R agonism, DIO mice were implanted with telemetric body temperature monitors and given a single subcutaneous injection of EB1002 (Fig. 2e). EB1002 administration led to a significant and sustained increase in oxygen consumption (Fig. 2f) and fatty acid oxidation (Fig. 2g) that was also reflected in a modest increase in core temperature (Fig. 2h). Concurrent with enhancing energy expenditure, a single administration of EB1002 also strongly decreased food intake (Fig. 2i) and respiratory exchange ratio (RER) (Fig. 2j) for more than 24 h. Collectively, these acute metabolic effects reduced body weight (Fig. 2k) without any overt signs of discomfort or changes in physical activity (Extended Data Fig. 2d). To further evaluate safety and toxicity, CD-1 mice were subjected to a dose escalation up to 7,500 nmol kg^{-1}. This dose amounted to more than 20 times the dose that we used in our mouse efficacy models. We did not observe any changes in serum liver enzymes (Extended Data Fig. 2e) or pathohistological signs (Extended Data Fig. 2f and Extended Data Table 4).

Consistent with previous knowledge of neurokinin biology[5], transient appearance of loose stools was observed at the highest doses and thus served to inform tolerance limits for EB1002 dosing. Notably, the efficacy of EB1002 was abolished both in genetic *Nk2r* knockout (Extended Data Fig. 2g–l) and after acute pharmacological NK2R antagonism (Fig. 2l–r), confirming robust in vivo selectivity.

We next investigated the effects of NK2R agonism on glucose metabolism. EB1002 significantly improved glucose tolerance in DIO mice 24 h after a single dose compared to mice that were either treated with vehicle only or treated with vehicle and pair-fed with EB1002-treated animals (Fig. 2s,t), showing that the glycaemic correction occurred independent of changes in insulin secretion or food intake reduction. To determine whether the improvement in glucose control was due to altered insulin sensitivity, we performed a hyperinsulinaemic–euglycaemic clamp study in chow-fed mice (Fig. 2u). Mice treated with a single dose of EB1002 required a 50% higher glucose infusion rate during steady state compared to vehicle controls (Fig. 2v and Extended Data Fig. 2m,n), revealing a profound increase in insulin sensitivity. EB1002 trended to enhance oxidative skeletal muscle glucose disposal (Extended Data Fig. 2o) and significantly increased glucose uptake into white adipose depots (Fig. 2w). However, NK2R-agonist-induced effects on white adipocyte glucose uptake or other metabolic functions, including oxygen consumption and lipolysis, were not cell autonomous (Extended Data Fig. 2p–r). We next sought to determine how NK2R agonism impacted tissue-specific insulin signalling in vivo. EB1002 acutely and significantly increased insulin-induced AKT phosphorylation in liver, gastrocnemius and brown adipose tissue (BAT) (Extended Data Fig. 2s–u). Despite the increased insulin-stimulated glucose uptake in WAT we observed during the clamp, there was no clear change in insulin-induced AKT phosphorylation in iWAT after EB1002 administration (Extended Data Fig. 2v). Together, these findings reveal that selective, long-acting NK2R agonism elicits dual regulation of energy expenditure and food intake and potently improves insulin sensitivity.

NK2R agonism improves metabolic health

Repeated daily administration of EB1002 significantly and sustainably reduced body weight (Fig. 3a and Extended Data Fig. 3a) at least in part owing to transient suppression of food intake (Fig. 3b) in DIO mice. Notably, injecting animals every other day with EB1002 was just as effective as daily administration at producing longer-term weight loss over

Table 4 | TWAS and sensitivity analysis of the association between *NK2R* expression and HbA1c levels in the ACB

Gene	TWAS		Sensitivity analysis		Trait
	Effect size	*P* value	Effect size	*P* value	
NK2R	−0.147312885	5.57322×10^{-48}	−0.13674113	1.75×10^{-7}	HbA1c
NK2R	−0.047902365	1.60712×10^{-14}	−0.05624646	2.29×10^{-2}	HbA1c (BMI-adjusted)
HK1	−0.005043655	0.647995	0.02991872	5.08×10^{-1}	HbA1c
HK1	0.000288765	0.9628904	−0.01008011	8.27×10^{-1}	HbA1c (BMI-adjusted)
TSPAN15	−0.032080736	0.004094338	−0.05479775	4.60×10^{-1}	HbA1c
TSPAN15	0.003103694	0.5906543	−0.01864292	9.05×10^{-1}	HbA1c (BMI-adjusted)

P values were calculated using a two-sided *z*-test. Since only three genes were considered, nominal *P* values without applying a genome-wide false-discovery rate correction are reported.
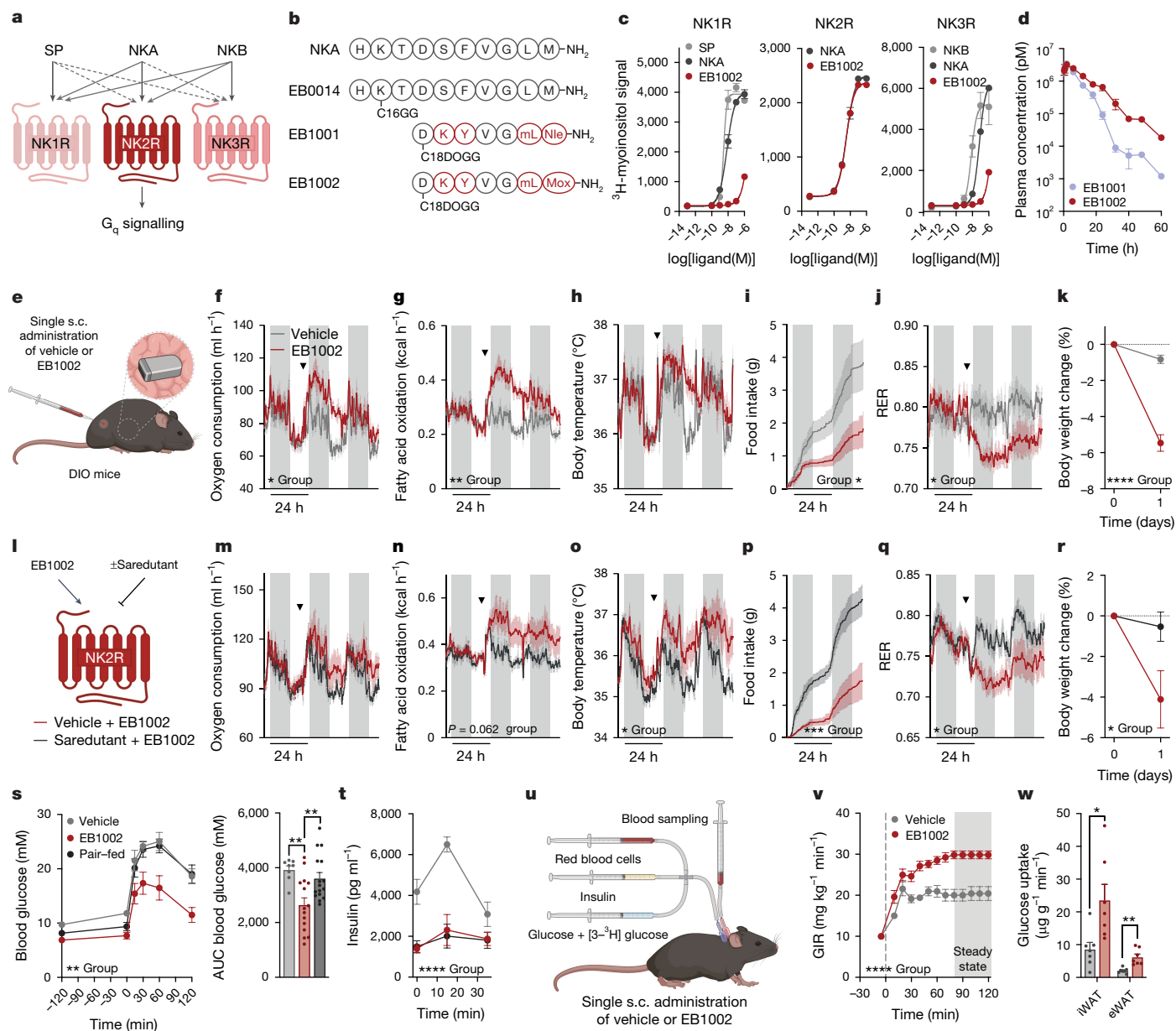
Fig. 2 | Development and characterization of first-in-class selective, long-acting NK2R agonists. a, Signalling schematic for the tachykinin receptor family along with respective endogenous ligands, substance P (SP), NKA and neurokinin B (NKB), adapted from ref. 6. **b**, Sequences of NKA and protracted, selective NK2R agonists. **c**, Ligand-induced Gq signalling of human tachykinin receptors in vitro (n = 2 per ligand). **d**, Pharmacokinetic profile of NK2R agonists (n = 3 mice per group). **e–k**, In vivo effects of a single injection of EB1002 (**e**; inset shows the implanted body temperature monitor) on oxygen consumption (**f**), fatty acid oxidation (**g**), body temperature (**h**), food intake (**i**), RER (**j**) and weight loss (**k**) in DIO mice. In **f–j**, arrowheads indicate time of injection of vehicle or EB1002. Plot colours in **f–k** match key in **f**. n = 6 (vehicle), n = 5 (EB1002) (**f–i**); n = 8 (vehicle), n = 9 (EB1002) (**k**). **l–r**, Evaluation of in vivo selectivity of EB1002 with or without pre-administration of the NK2R antagonist saredutant

in DIO mice (**l**) on oxygen consumption (**m**), fatty acid oxidation (**n**), body temperature (**o**), food intake (**p**), RER (**q**) and weight loss (**r**). In **m–q**, arrowheads indicate 0.5 h pretreatment with vehicle or saredutant followed by EB1002. Plot colours in **m–r** match key below **l**. n = 6 per group (**m,n,p–r**); n = 5 per group (**o**). **s,t**, Glucose tolerance (**s**) and insulin level (**t**) of DIO mice (n = 8 (vehicle), n = 15 (325 nmol kg⁻¹ EB1002), n = 16 (pair-fed with the EB1002-treated group)). **u**, Setup of the hyperinsulinaemic–euglycaemic clamp study. **v,w**, Glucose infusion rate (GIR) (**v**) and glucose uptake into iWAT and eWAT depots (**w**), for a hyperinsulinaemic–euglycaemic clamp of lean mice 16 h after a single injection of vehicle (n = 7) or EB1002 (n = 8). Data are mean ± s.e.m. *P < 0.05, **P < 0.01, ***P < 0.005, ****P < 0.0001. Detailed statistics are in the Supplementary Information and Source Data.

the course of 21 days (Extended Data Fig. 3a). However, we observed that the body weights of NK2R-treated animals began to increase gradually over the 21 days of injections, raising potential concerns of desensitization (Extended Data Fig. 3a). Thus, we tracked the weight re-gain of the cohort after injections were ceased and then re-administered a single injection of EB1002 to all mice (Extended Data Fig. 3b). Regardless of previous compound exposure, all mice exhibited similar weight loss (Extended Data Fig. 3b,c), demonstrating that there was no lasting

desensitization induced by systemic NK2R agonism. Unexpectedly, the single injection of EB1002 resulted in 10–15% weight loss over 7 days (Extended Data Fig. 3c), suggesting a far more sustained efficacy than predicted by blood occupancy of the peptide.

In the initial phase of systemic agonism, we found that EB1002 acutely increased faecal triglyceride content and trended to increase faecal cholesterol (Extended Data Fig. 3d,e), suggesting a potential for reduced lipid absorption and/or an induced release of lipids into the

Fig. 3 | Improvement of systemic energy homeostasis by long-acting NK2R agonism. a,b, Weight loss (**a**) and food intake (**b**) of DIO mice injected daily with vehicle or EB1002 (*n* = 6 per group). WT, wild type. **c,** Weight loss of DIO mice that were transitioned to chow diet or continued on HFD 5 days before daily injections (*n* = 6 (HFD vehicle), *n* = 8 (chow vehicle, chow EB1002 and HFD EB1002)). Arrowhead indicates first injection. **d–g,** Plasma concentrations of GLP-1 (**d**), leptin (**e**), glucagon (**f**) and PYY (**g**) of DIO mice injected daily with vehicle (*n* = 7) or EB1002 (*n* = 8). **h,** Body composition of DIO mice injected daily with vehicle (*n* = 11) or EB1002 (*n* = 15). **i–k,** Weight loss (**i**), food intake (**j**) and body composition (**k**) of DIO *Nk2r*-knockout (KO) mice injected daily with vehicle (*n* = 8) or EB1002 (*n* = 9). **l,** Weight loss of DIO mice injected daily with vehicle (*n* = 11), EB1002 (*n* = 15) or vehicle and pair-fed with EB1002-treated mice (*n* = 12). **m–t,** Schematic of DIO *Ucp1*-knockout mice at thermoneutrality (**m**) used to assess weight loss (**n**), blood glucose concentration (**o**), RER (**p**),

fatty acid oxidation (**q**) and oxygen consumption (**r**), and linear regression of oxygen consumption versus body weight (**s**) and body temperature (**t**) after a single injection of vehicle, EB1002 or vehicle and pair-fed with EB1002-treated mice. In **p–r,t,** arrowheads indicate time of injection, diamonds indicate replenishment of food for the pair-fed group. In **n–t,** *n* = 6 per group. **u,v,** Weight loss (**u**) and food intake (**v**) of DIO, thermoneutrally housed *Ucp1*-knockout mice injected daily with vehicle (*n* = 6) or EB1002 (*n* = 7). **w–z,** Setup of triple-chip study to investigate the anatomical resolution of thermogenic output (**w**) with interscapular temperature (**x**; *n* = 3), hindlimb temperature (**y**; *n* = 5) and abdominal temperature (**z**; *n* = 5) of DIO mice after a single injection of EB1002 (indicated by arrowheads (**x–z**)). Data are mean ± s.e.m. *$P < 0.05$, **$P < 0.01$, ***$P < 0.005$, ****$P < 0.0001$. Detailed statistics are in the Supplementary Information and Source Data.

intestine. Moreover, the efficacy of NK2R agonism was not dependent on ingestion of high-fat diet (HFD), as DIO mice that were transitioned from HFD to chow diet 5 days before EB1002 treatment to mimic a dietary intervention, displayed similar weight loss to mice that were maintained on HFD (Fig. 3c and Extended Data Fig. 3f). We next investigated whether acute or repeated administration of an NK2R agonist affected the blood levels of hormones known to modulate feeding

and metabolism. A single injection of EB1002 did not change the concentrations of GLP-1, leptin, glucagon or peptide YY (PYY) (Fig. 3d–g). However, leptin and glucagon were significantly decreased and PYY was significantly increased following a week of daily injections (Fig. 3d–g), suggesting that NK2R-agonist-induced whole-body metabolic improvements engage other homeostatic-regulating hormone pathways.

Article

Body composition was assessed after 7 days of daily injections to determine the cause of the weight reduction. We found that NK2R-agonist-induced weight loss was solely attributable to decreased adiposity (Fig. 3h and Extended Data Fig. 3g) whereas lean mass was spared (Fig. 3h). There were no sex-dependent differences in response to NK2R agonism as EB1002-treated female DIO mice displayed similar changes in body weight, body composition, adipose depot weights, acute blood glucose control, food intake, RER, oxygen consumption, fatty acid oxidation and body temperature (Extended Data Fig. 3h–p). The effects of repeated daily EB1002 injections were abolished in animals lacking *Nk2r* (Fig. 3i–k and Extended Data Fig. 3q), reinforcing the selectivity of the agonist. The dependence of NK2R-agonist-mediated weight loss on both food intake (Fig. 2i) and energy-expending mechanisms (Fig. 2f), was further evidenced when comparing EB1002-treated animals to pair-fed controls (Fig. 3l).

The translational potential of energy-expending modes-of-action can be confounded by the reliance of rodent physiology on BAT thermogenesis. Therefore, we evaluated the efficacy of NK2R agonism in thermoneutrally housed DIO mice lacking the canonical BAT effector, uncoupling protein 1 (UCP1) (Fig. 3m). To distinguish effects from reduced food intake versus increased energy expenditure, we included a pair-fed *Ucp1*-knockout group that was matched to EB1002-treated mice. In DIO *Ucp1*-knockout mice, acute EB1002 treatment significantly reduced body weight and blood glucose compared to vehicle-injected and pair-fed mice (Fig. 3n,o), demonstrating NK2R agonism elicited UCP1-independent mechanisms of weight loss and glucose control. A single EB1002 injection into mice lacking *Ucp1* reduced RER more robustly than pair feeding over 2 days (Fig. 3p) and increased fatty acid oxidation (Fig. 3q), oxygen consumption (Fig. 3r,s) and body temperature (Fig. 3t). The observation that oxygen consumption and body temperature of pair-fed mice were lower than those of the the vehicle group suggested that EB1002 induced an even greater degree of energy expenditure than previously estimated. Repeated daily injections of EB1002 in DIO *Ucp1*-knockout mice at thermoneutrality reduced weight and food intake (Fig. 3u,v) to similar magnitudes as our earlier studies in wild-type mice.

We next sought to investigate the anatomical contributions and dynamics of NK2R-induced energy expenditure. Whereas our standardized in vivo model involves implanting temperature probes that are free-moving throughout the peritoneal cavity, we surgically anchored telemetric temperature probes to three regions of each mouse to achieve spatial resolution (Fig. 3w): (1) embedded in the interscapular region, between the brown adipose tissue and shoulder muscles; (2) positioned along the upper thigh, running parallel to the quadriceps muscle; and (3) situated against the abdominal wall of the peritoneal cavity. Interscapular BAT depots were surgically denervated in a subset of the mice. Compared with vehicle injection in the same mice, a single subcutaneous injection of EB1002 robustly increased interscapular temperature acutely and continuously over 48 h (Fig. 3x and Extended Data Fig. 3r). However, hindlimb temperature was initially blunted before progressively increasing between 2 and 5 days after injection (Fig. 3y and Extended Data Fig. 3s), revealing a multiphasic, temporal distribution of thermogenic output. Abdominal temperature was initially blunted before returning to the pre-injection pattern (Fig. 3z and Extended Data Fig. 3t). Similar patterns in all three anatomical regions were observed in the BAT-denervated mice (Extended Data Fig. 3u–y). Although it remains unclear how NK2R agonism orchestrates the observed anatomical and temporal dynamics, the ability of a single administration of EB1002 to impart effects over the course of a week is in line with the timeframe of earlier weight loss studies in which one injection led to progressive weight reduction over 7 days (Extended Data Fig. 3b,c). Collectively, these findings show that long-acting NK2R-induced improvements in metabolic outcomes are driven by both reduced food intake and increased energy expenditure, which occurs dynamically across multiple tissues and independently of the canonical BAT activity.

NK2R agonism in the CNS and periphery

We next assessed NK2R agonism in the context of genetic obesity and canonical hypothalamic appetite-regulating circuitry[35,36]. EB1002 was subcutaneously administered to DIO mice or hyperphagic models lacking leptin (*ob*/*ob*) or the melanocortin 4 receptor (*Mc4r*-knockout) (Extended Data Fig. 4a). Surprisingly, the same dose of EB1002 (325 nmol kg^{-1}) that moderately lowered food intake in non-hyperphagic DIO mice robustly attenuated appetite in both male and female *ob*/*ob* mice (Extended Data Fig. 4b,), indicating that NK2R agonism not only regulates food intake independently of leptin signalling but also seems to be potentiated in the absence of leptin. However, this potentiated action of NK2R agonism was not observed in mice lacking *Mc4r* (Extended Data Fig. 4b), suggesting that NK2R food intake regulation was still, to some extent, dependent on canonical appetite-regulating signalling downstream of leptin. The markedly increased efficacy of NK2R agonism in leptin-deficient mice was also reflected in body weight (Extended Data Fig. 4c) and blood glucose (Extended Data Fig. 4d), which were sustained significantly lower even 48 h after injection despite food intake beginning to increase back towards baseline (Extended Data Fig. 4e).

To distinguish between peripheral and central contributions of NK2R signalling, we performed a pharmacological study comparing subcutaneous and intracerebroventricular (ICV) administration of EB1002. HFD-fed *ob*/*ob* mice were housed in indirect calorimetric cages at thermoneutrality and metabolic readouts were assessed after a single subcutaneous injection of vehicle or EB1002. After wash-out, the mice received an ICV dose in a crossover design (Fig. 4a and Extended Data Fig. 4f). Central delivery of EB1002 robustly reduced food intake (Fig. 4b) and RER (Extended Data Fig. 4g) similarly to peripheral administration, indicating that appetite could be directly controlled by the CNS. However, ICV delivery of EB1002 significantly decreased oxygen consumption (Fig. 4c), consistent with an effect primarily on food intake without a simultaneous boosting or maintenance of energy expenditure as was observed following subcutaneous injection (Fig. 4c). In line with the oxygen consumption measurements, body temperature was more robustly increased by subcutaneous injection compared with ICV delivery, yet central administration was still able to elicit a distinct temperature increase during the light phase (Extended Data Fig. 4h). Thus, thermogenic contributions of NK2R signalling appear to emanate largely from peripherally accessible regions but direct contributions from the CNS cannot be entirely ruled out. Even without inducing energy expenditure, the EB1002 dose delivered centrally produced weight reductions similar to peripheral dosing (Fig. 4d), probably owing to the more marked suppression of food intake. Notably however, blood glucose was only significantly decreased by subcutaneous administration (Fig. 4e), suggesting that acute glycaemic control was weight-independent and required peripheral NK2R signalling. The effects of the ICV dose were CNS-specific as peripheral administration of the ICV concentration, equivalent to 40 nmol kg^{-1}, elicited no effects on metabolic parameters (Extended Data Fig. 4i–m). These findings collectively suggest that NK2R activation acts via the periphery and CNS to simultaneously suppress appetite, increase energy expenditure and improve insulin sensitivity.

We next sought to gain insight into which brain regions might contribute to the NK2R-mediated suppression of feeding. We found that administration of EB1002 acutely and significantly reduced food intake during refeeding following an overnight fast (Extended Data Fig. 5a). Given that the activity of Agouti-related peptide-expressing neurons (AgRP neurons) mediates a significant portion of refeeding, this result suggests that EB1002 could, at least in part, overcome AgRP neuron-driven feeding. The activity of AgRP neurons can be blocked through the activation of neurons in the dorsomedial hypothalamus (DMH) or the dorsal vagal complex (DVC). To evaluate the potential activation of these sites (as well as other regions known to regulate
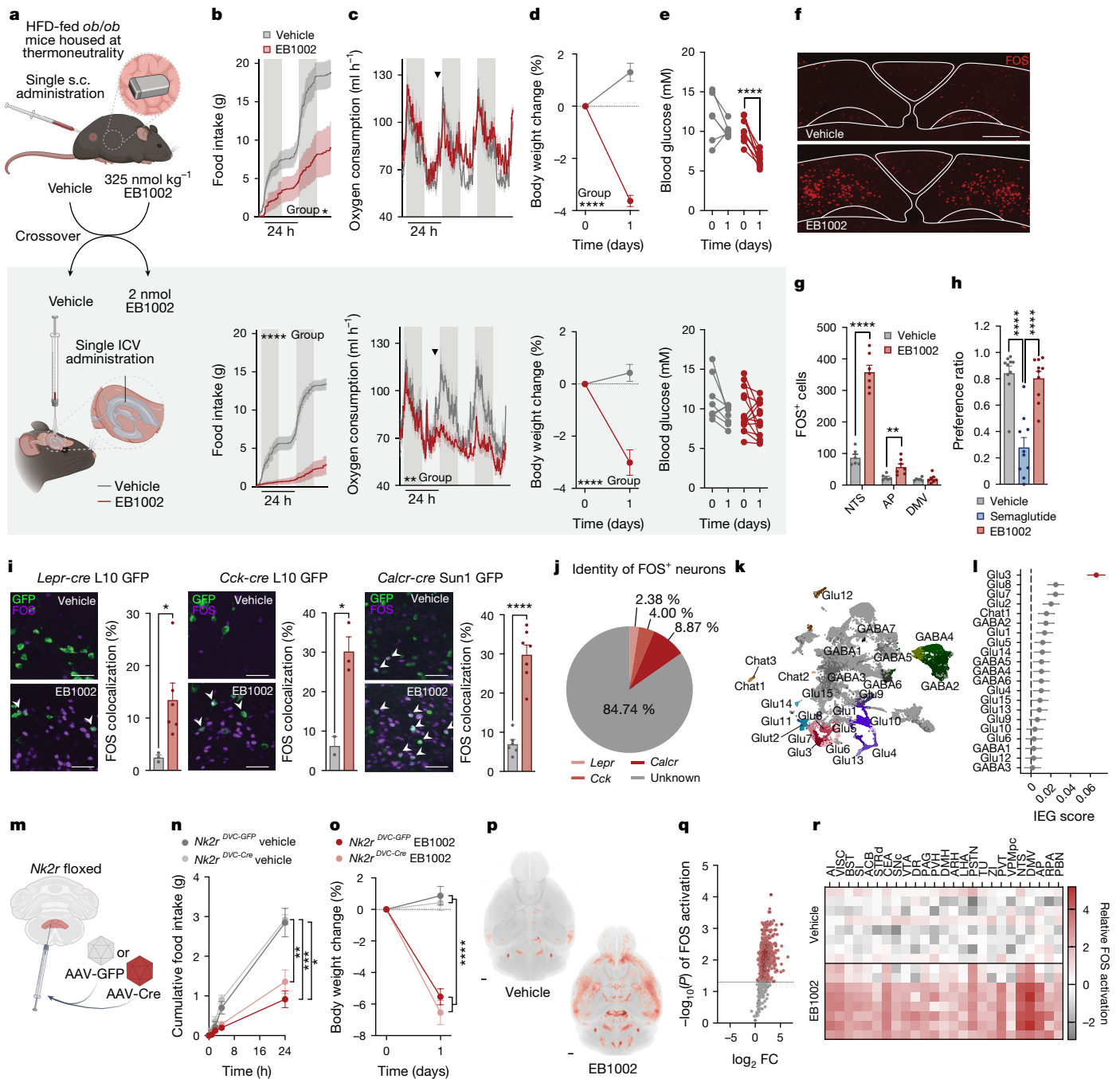
Fig. 4 | Distinct central and peripheral actions of long-acting NK2R agonism.
a, Study design comparing effects of central and peripheral delivery of EB1002.
b–**e**, Food intake (**b**), oxygen consumption (**c**), weight loss (**d**) and blood glucose concentration (**e**) following subcutaneous or ICV injection (all plot colours as in key in **b**). $n = 6$ (vehicle subcutaneous injections, EB1002 ICV injections), $n = 4$ (EB1002 subcutaneous injections, vehicle ICV injections) (**b**,**c**); $n = 6$ (vehicle subcutaneous injections), $n = 10$ (EB1002 subcutaneous injections), $n = 8$ (vehicle ICV injections), $n = 13$ (EB1002 ICV injections) (**d**,**e**). Arrowheads indicate injections (**c**). **f**,**g**, Representative FOS staining in the DVC (**f**; scale bar, 200 μm) and quantification of FOS-positive cells in the NTS, AP and DMV (**g**) of mice injected with vehicle ($n = 6$) or EB1002 ($n = 8$). **h**, Preference ratio for vehicle, semaglutide or EB1002 ($n = 10$ per group). **i**, Representative microscopy images and quantification of FOS colocalization with reporter neurons expressing GFP in the NTS of *Lepr*^{cre} L10 GFP ($n = 3$ (vehicle), $n = 6$ (EB1002)), *Cck*^{cre} L10 GFP ($n = 2$ (vehicle), $n = 3$ (EB1002)) and *Calcr*^{cre} Sun1 GFP mice ($n = 6$ (vehicle), $n = 7$ (EB1002))

injected with vehicle or EB1002. Scale bars, 50 μm. Plot colours as in key in **b**.
j, Identity of FOS⁺ neurons in the NTS of EB1002-injected mice. **k**, Uniform manifold approximation and projection (UMAP) plot of expression data from 23,664 neurons coloured by populations according to ref. 39. **l**, Immediate early gene (IEG) expression in DVC snRNA-seq data from mice injected with vehicle or EB1002 ($n = 6$ samples with 5 mice per sample). **m**, Schematic of AAV injection into the DVC of *Nk2r*-floxed mice. **n**,**o**, Food intake (**n**) and weight loss (**o**) of *Nk2r*$^{DVC-GFP}$ and *Nk2r*$^{DVC-cre}$ mice injected with vehicle or EB1002 ($n = 5$ per group). **p**–**r**, Group average FOS heat map (**p**; scale bar, 500 μm), volcano plot of brain subregions (**q**) and heat map of activated brain regions involved in feeding, energy expenditure and reward (**r**) of wild-type DIO mice injected with vehicle or EB1002 ($n = 8$ per group). Data in **j** are mean, and data in all other graphs are mean ± s.e.m. *$P < 0.05$, **$P < 0.01$, ***$P < 0.005$, ****$P < 0.0001$. Detailed statistics are in the Supplementary Information and Source Data.

Article

food intake, including the paraventricular nucleus of the hypothalamus (PVH), arcuate nucleus (ARH) and the parabrachial nucleus (PBN)), we assessed FOS immunoreactivity (FOS-IR) 2 h after EB1002 administration in overnight-fasted mice. NK2R-agonist-induced changes in FOS-IR were detected only in the DVC (Extended Data Fig. 5b,c). Within this region, FOS-IR was primarily increased in neurons within the nucleus of the solitary tract (NTS) and to a lower extent in the area postrema (AP); we found no change in the dorsal motor nucleus of the vagus (DMV) (Fig. 4f,g). Whereas the AP and NTS each restrain food intake as part of the physiological response to a meal, some AP and NTS neurons also promote aversive signals[37,38]. Thus, we performed a saccharin-based conditioned taste avoidance test with EB1002 treatment, revealing no conditioned taste aversion formation by NK2R agonism (unlike the aversive GLP-1R agonist semaglutide) (Fig. 4h). We additionally assessed gastric emptying rate (also modulated by the DVC) but found no difference following acute administration of EB1002 when compared to vehicle (Extended Data Fig. 5d). Thus, although EB1002 activates neurons in the DVC, the appetite suppression by the compound appears to occur independently of aversive responses or alterations in gastric emptying.

To map which neuronal populations in the DVC were activated by NK2R agonism, we used reporter mice that labelled *Lepr-*, *Cck-* or *Calcr*-expressing neurons. Whereas EB1002 activated a subset of neurons within these established hunger-regulating populations (Fig. 4i and Extended Data Fig. 5e–g), the majority of FOS-positive neurons were distinct from these canonical populations (Fig. 4j). To further characterize the cellular identity of DVC neurons activated by EB1002, we generated a single-nucleus RNA-sequencing (snRNA-seq) dataset of the DVC from vehicle- and EB1002-treated mice. Transcriptionally defined cell classes were identified with known neuronal and glial markers. The neuronal population was subclassified and labelled on the basis of a publicly available DVC atlas[39], and 23,664 nuclei were categorized into 25 neuronal populations (Fig. 4k). Cells from both treatment groups were evenly distributed across all neuronal clusters (Extended Data Fig. 5h). Quantification of immediate early gene expression and transcriptional differences revealed Glu3 neurons[39], a *Gal-* and *Lepr*-expressing population of glutamatergic NTS neurons (Extended Data Fig. 4i), to be the most responsive to EB1002 (Fig. 4l and Extended Data Fig. 5j).

Given that *Nk2r* is expressed in the NTS (Extended Data Fig. 5k) and ICV administration strongly regulated food intake (Fig. 4b), we assessed the importance of *Nkr2* expression in the DVC for the response to EB1002. We directly injected GFP- or Cre-expressing adeno-associated virus (AAV) into the DVC of *Nk2r*-floxed mice (Fig. 4m and Extended Data Fig. 5l) (called *Nk2r^DVC-GFP* or *Nk2r^DVC-cre*, respectively, here) and found that EB1002 was still able to acutely suppress food intake and reduce body weight in *Nk2r^DVC-cre* mice (Fig. 4n,o). Although we observed a trend towards increased cell death in the AAV-Cre-injected DVCs compared with AAV-GFP controls (Extended Data Fig. 5m), the preservation of EB1002 effects in these mice suggests that direct NK2R signalling in the DVC is not required for the efficacy of systemic NK2R agonism. These data do not preclude the possibility that NTS neurons, which would be downstream from a peripheral NK2R-induced signal, might mediate EB1002 action.

To comprehensively decode the CNS contributions of NK2R agonism in a global, unbiased manner, we next resolved whole-brain FOS activation using iDISCO (immunolabelling-enabled three-dimensional imaging of solvent-cleared organs) imaging after a peripheral administration of vehicle or EB1002, using DIO mice fasted for the 2 h dosing period (as opposed to the overnight-fasted chow-fed mice in Fig. 4f,g and Extended Data Fig. 5b,c). This analysis revealed the widespread activation of FOS by EB1002 compared with vehicle (Fig. 4p,q), suggesting potentially different responses to NK2R agonism for obese mice compared with lean mice. In DIO mice, EB1002 stimulated FOS activation in many brain regions involved in the control of food intake, reward and

energy balance and/or targeted by clinically validated weight-lowering drugs[40], including, but not limited to, the PVH, NTS, AP, DMV, PBN, ARH, DMH, ACB, lateral hypothalamic area (LHA) and parasubthalamic nucleus (PSTN) (Fig. 4r). The effect of EB1002 further extended to the ventral and lateral areas of the cortical plate (Fig. 4r), which are associated with the processing of olfactory and taste information, consistent with a potential role of NK2R agonism on sensory processing related to food intake. These complex networks of NK2R action in the CNS suggest that long-acting NK2R agonism exerts systemic control through the coordinated engagement of numerous homeostasis and behaviour-regulating neuronal populations.

Effects of NK2R agonism in primates

In light of translational hurdles between rodents and higher mammals, we next sought to explore NK2R agonism in a cohort of obese male and female rhesus macaques (nonhuman primates) with cardiometabolic disease. At the time when the macaque study was initiated, EB1001 was the most advanced NK2R agonist developed, and was therefore the compound selected. EB1001 was administered daily through subcutaneous injection in a dose-escalation study design over eight weeks to determine tolerability and explore potential efficacy (Fig. 5a). The dosing period was followed by a two-week wash-out period. To our knowledge, selective NK2R agonism has not previously been tested in nonhuman primates, and the neurokinin receptor family has been linked to several adverse side effects[5]. Therefore, a dedicated primate behavioural specialist monitored the animals throughout the study, and compound exposure was assessed at each dose (Extended Data Fig. 6a). In line with most obesity and T2D therapeutic agents, gastrointestinal events were the primary side effects. Although there were no incidents of nausea, emesis or diarrhoea at any dose, there was a peak in looser stools at the highest dose of 480 nmol kg^{-1} (Extended Data Fig. 6b), along with a concurrent spike in subdued, withdrawn behaviour (Extended Data Fig. 6c). Gastrointestinal effects abruptly ceased after a return to the preceding tolerated dose of 240 nmol kg^{-1}, suggesting a profile driven by maximum serum concentration (C_{max}), and withdrawn behaviour followed similarly. Importantly, there were no indications of anxiety or anxiety-like behaviours (for example, agitation, pacing or unrest) at any dose (Fig. 5b). Moreover, there was no adverse effect on cardiopulmonary (Fig. 5c and Extended Data Fig. 6d), hepatic (Fig. 5d and Extended Data Fig. 6e) or renal (Extended Data Fig. 6f) parameters. Thus, these dose-escalation findings establish a safety window for evaluating NK2R agonism in obese macaques.

Even using the early generation tool peptide EB1001, we were able to gain insights into the potential efficacy of NK2R agonism in macaques. Notably, although all macaques in the cohort were obese, their glucose control varied from normoglycaemic to a range across the diabetes spectrum, from mild to severe insulin resistance (stratified by criteria adapted from ref. 41) (Fig. 5e). Over the course of the eight-week dose-up, EB1001 led to a modest but significant reduction in body weight across the whole cohort (Extended Data Fig. 6g), which was driven by non-plateauing weight loss in the diabetic group that was maintained throughout the two-week period following treatment cessation (Fig. 5f). After an initial trending difference in food intake between normoglycaemic and diabetic animals (Fig. 5g), all macaques uniformly exhibited an approximate 25% decrease in food intake (Extended Data Fig. 6h). Technical limitations prevented the measurement of energy expenditure in the macaques.

Nonetheless, despite not being able to determine the maximal weight-lowering potential of NK2R agonism by the conclusion of the study, there were several improvements in cardiometabolic parameters. Before reaching the full extent of weight loss, EB1001 markedly reduced fasting blood glucose concentrations (Fig. 5h) and insulin levels (Fig. 5i), leading to a uniform correction of insulin resistance (as assessed by homeostatic model assessment–insulin resistance (HOMA-IR)) (Fig. 5j)
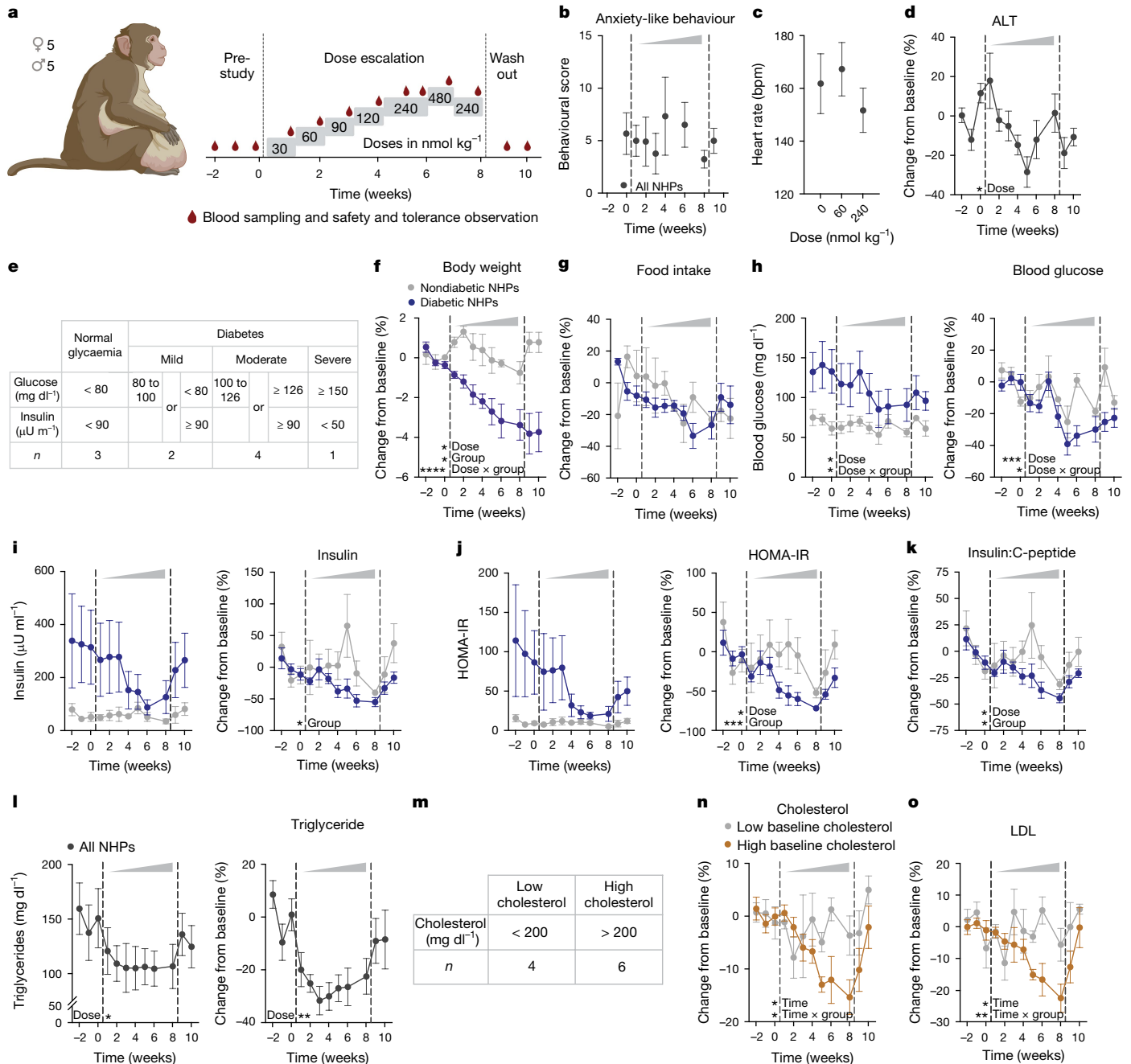
Fig. 5 | NK2R agonism safely counteracts cardiometabolic disease in diabetic, obese macaques. a, Schematic of EB1001 dose-escalation study in rhesus macaques (nonhuman primates (NHPs)). **b**–**d**, Anxiety-like behaviour (**b**), heart rate (**c**) and blood alanine transaminase concentration over the course of the dose-escalation study (*n* = 10 macaques). **e**, Stratification of macaque groups on the basis of diabetic status. **f**–**k**, Changes in body weight (**f**), food intake (**g**), fasting blood glucose (**h**), insulin level (**i**), HOMA-IR (**j**) and insulin:C-peptide ratio (**k**) for normoglycaemic (*n* = 3) and diabetic (*n* = 7) macaques. All plot colours as in key in **f**. **l**, Changes in triglyceride concentrations for all macaques over the course of the study (*n* = 10 macaques). **m**–**o**, Stratification of macaque groups on the basis of baseline cholesterol levels (**m**) and changes in total cholesterol (**n**) and LDL cholesterol (**o**) over the course of the dose escalation. All plot colours as in **n**. *n* = 4 macaques (low baseline cholesterol), *n* = 6 macaques (high baseline cholesterol). Data are mean ± s.e.m. *P < 0.05, **P < 0.01, ***P < 0.005, ****P < 0.0001. Detailed statistics are in the Supplementary Information and Source Data.

across the heterogenous diabetic group of macaques. These findings on glucose control underscore the genetic association that we uncovered between *NK2R* variants and HbA1c levels in humans. Notably, the improvements in glucose control were still present two weeks after the final compound dosing. Despite the marked improvement in glucose control, NK2R agonism did not produce any incidents of hypoglycaemia in the macaques at any point during the dose escalation. In addition, the insulin:C-peptide ratio, a non-invasive indicator of hepatic steatosis[42], was also significantly decreased in diabetic macaques following EB1001

administration (Fig. 5k), suggesting an NK2R-agonist-induced reduction in liver fat. In line with these results, EB1001 rapidly and robustly lowered plasma triglycerides in all macaques (Fig. 5l), irrespective of diabetic status (Extended Data Fig. 6i). Furthermore, NK2R agonism significantly reduced both total and low-density lipoprotein (LDL) cholesterol in animals with high starting cholesterol (Fig. 5m–o) (as stratified by ref. 43). Together, in obese, diabetic macaques, NK2R agonism decreased body weight and food intake without causing emesis, and efficiently improved insulin sensitivity and lipid control. The weight

Article

loss and glucose control appeared to be even more pronounced in the diabetic macaques. Notably, the efficacy parameters and side-effect profile of NK2R agonism that were assessed in mice and macaques were fully translatable (Extended Data Fig. 6j).

Discussion

We set out to identify GPCR pathways that regulate energy homeostasis and could be leveraged to improve cardiometabolic health. In our search, we uncovered a novel drug target whereby agonism of NK2R elicited increased peripheral energy expenditure and insulin sensitization, as well as central control of appetite. Our motivation to design selective NK2R agonists was inspired by the revelation of genetic associations to obesity and HbA1c. The association of HbA1c with *NK2R* variants appears to have been previously overshadowed by the neighbouring gene *HK1*. Given the strength of the association between HbA1c and *HK1* variants[26] and the close genomic proximity of *HK1* and *NK2R*, fully disentangling variant associations between these two genes is difficult. Nevertheless, our fine-mapping analysis and TWASs revealed associations between HbA1c and *NK2R* that were independent of *HK1* variants. Notably, the HbA1c associations in the *HK1–NK2R–TSPAN15* region have not been ascribed to glycaemic control, but are instead linked to haemoglobin biology by affecting the turnover or metabolism of erythrocytes[44]. To that end, the anaemic phenotype of mice that are deficient in *Hk1* (ref. 45) is fully consistent with this nonglycaemic influence on HbA1c. However, NK2R agonism significantly counteracted hyperglycaemia and improved insulin sensitivity acutely in mice and chronically in macaques, suggesting that NK2R signalling acts on glucose control and not on erythrocyte viability. Further supporting the erythrocyte independence of NK2R action are the findings that blood oxygenation was significantly improved and blood urea nitrogen remained stable in macaques after prolonged NK2R-agonist administration. This genomic region has also been previously linked to cholesterol[27], which is less likely to be attributed to the erythrocyte-based, proanaemic outcome elicited by HK1 deficiency. NK2R agonism lowered triglycerides in all macaques and significantly decreased LDL cholesterol in macaques with higher baseline cholesterol, hinting that *NK2R* may potentially be the gene responsible for this association to this region.

Key questions raised by the genetic findings include what the mechanistic underpinnings are of the obesity association with *NK2R* variants found in the Greenlanders, and why this pattern is not observed in the Western European population. Similarly, why is the HbA1c association found in Western Europeans and not in Greenlanders? It is, of course, tempting to speculate that the pronounced differences in diet and environment may be contributing factors. Moreover, on the basis of the extensive understanding of the genetics of human obesity[46,47], the effect sizes of the reported *NK2R* variant imply that disruption of NK2R signalling does not have a causal pathophysiological role in the development of obesity. However, the generation of long-acting, potent NK2R agonists raises the possibility that sustained pharmacological activation may ultimately contribute meaningfully to weight management in humans, regardless of the physiological role of this receptor. Future investigation into the mode of action of NK2R and comparison between pharmacological and physiological contributions to energy homeostasis should provide clarifying insights.

Owing to the high bar set by current and late-stage pipeline strategies for the treatment of obesity[2], for which more than 20% weight loss in humans is now achievable[13,48], the modest weight loss and the gastrointestinal-related tolerability ceiling observed in preclinical studies of these nonoptimized NK2R agonists would probably limit the standalone targeting of this receptor for cardiometabolic indications. This prospect is made even more likely in light of the profound recent advances and an overall shift to leveraging multiple modes of action in unimolecular polyagonists[2], exemplified by clinically validated compounds such as tirzepatide (acting on GLP-1 and GIP[13], with average weight loss of up to 20.9%), survodutide (acting on GLP-1 and GCG[49], with average weight loss of up to 14.9%) and retatrutide (acting on GLP-1, GIP and GCG[48], with average weight loss of up to 22.1%). In the context of polyagonism, the energy-expending feature of NK2R agonism could provide an attractive alternative to glucagon, given that in preclinical models, NK2R agonism increased oxygen consumption but did not affect heart rate and spared lean mass. Moreover, the non-aversive appetite suppression, weight-lowering efficacy and insulin sensitization in diabetic obese animals would represent additional strengths over the current pharmaceutical toolkit. Thus, polyagonism strategies that incorporate NK2R activation may provide the greatest opportunity to exploit this new biology for next-generation biopharmaceuticals.

This work reveals the beneficial effects of pharmacological NK2R activation, but the physiological roles of NK2R signalling in metabolism are likely to be more nuanced and complex. Native NKA has a half-life on the order of minutes[5] and is cleared with high efficiency that prevents appreciable circulation. Thus, endogenous NK2R signalling is largely dictated by local paracrine actions of NKA released from resident secretory cells. Conversely, EB1001 and EB1002 are present in circulation for hours and will theoretically activate all accessible NK2R receptors throughout the body. To that end, the collective effects of EB1001 or EB1002-induced central anorexigenic control and peripheral increase in energy expenditure and insulin sensitivity may be physiologically elicited separately by NKA–NK2R signalling axes in different organ systems and biological contexts. Specifically, determining whether peripheral energy expenditure and central anorectic control are coordinated together and functionally linked will be a critical point to resolve how endogenous NK2R signalling affects systemic energy homeostasis. From a therapeutic standpoint, it will be further advantageous to mechanistically delineate how the beneficial cardiometabolic and gastrointestinal effects are regulated. The dose-escalation study in macaques supports a pharmacological model whereby cardiometabolic efficacy parameters are largely dictated by compound exposure, whereas effects on the gastrointestinal are driven by C_{max}. Notably, although leveraging exposure-driven efficacy and minimizing gastrointestinal motility is essential for the cardiometabolic therapeutic window, efforts to capitalize on the acute, high-dose effects are being targeted as a potential way to help restore gut motility in individuals who have undergone spinal cord trauma and suffer from diminished neuronal control of gastrointestinal function. Therefore, resolving the complex cell, tissue and interorgan contributions that collectively shape the whole-body responses to physiological and pharmacological NK2R activation could enable us to clinically harness the full potential of NK2R biology across indications.

Another key, outstanding question surrounding the mode of action of NK2R is which tissue or tissues are responsible for the energy expenditure. NK2R is expressed throughout the body, however, the current understanding of NKA action is centred largely around its role as a local, non-circulating messenger in the gastrointestinal tract or as a neurotransmitter in the CNS. Given that we find white adipose depots to be the organs with the most significant NK2R-agonist-induced glucose disposal, and previous work in *Caenorhabditis elegans* has implicated NK2R signalling in adipose catabolism[50], these tissues represent intriguing candidates. Palamiuc et al. also found that *C. elegans* tachykinin signalling functionally interacted with central serotonergic signalling[50], which is known to influence catabolic pathways and holds considerable potential for the treatment of cardiometabolic disease[51]. The lack of direct effect of NK2R agonists on isolated adipocytes suggests the requirement for other cell types or interactions (for example, innervation) in the in vivo tissue environment. Moreover, the anatomical and temporal resolution of NK2R-agonist-induced effects on heat production implicate contributions from multiple organs at different times following compound administration. However, our findings from BAT-denervated animals and thermoneutrally housed *Ucp1*-knockout mice probably preclude a role of canonical brown adipocytes.

The ability of EB1002-mediated NK2R agonism to suppress food intake and body weight in *ob/ob* mice, which are obese owing to CNS alterations in appetite control, together with the ability of ICV-delivered EB1002 to reduce feeding and body weight, reveal the importance of NK2R-regulated CNS pathways for the salient actions of EB1002. The important task of defining the neural systems by which NK2R signalling acts to control metabolism and food intake will require substantial additional work, however. Although neurons in the DVC (especially the NTS) were most strongly activated by EB1002 under multiple conditions and we identified several NTS cell types that were activated by EB1002, ablating *Nk2r* in the DVC did not affect EB1002-induced appetite suppression and weight loss. Consistently, iDISCO imaging of whole brains from EB1002-treated DIO mice revealed that NK2R agonism elicited FOS activation in many brain regions (including in many areas linked to appetite, energy expenditure, body weight regulation, reward and the processing of olfactory and taste information). Although one or more of these brain regions presumably mediate the effects of EB1002 on energy balance, the lack of strong detection and spatial resolution of *Nk2r* expression data in the CNS from single-nuclei RNA-sequencing brain atlases render it unclear how much of the NK2R-dependent FOS activation is due to afferent signals conveyed from the periphery, direct action on neurons in a particular brain region, or signalling between interconnected CNS regions. Furthermore, our studies were all performed using a 2 h timepoint, when EB1002 is maximally high in the blood. Thus, future investigations to map *Nk2r* and FOS co-expression and incorporating multiple timepoints may better decode the cell types and complex trajectory of neuronal signalling that mediate NK2R control of energy homeostasis.

Given the sexual dimorphism present in cardiovascular metabolism linked to body weight and energy homeostasis[52] and the translational blind spots in exclusively testing new therapeutic mechanisms in male preclinical models[53], we evaluated key features of NK2R agonism in female DIO mice. Effects on body weight, blood glucose, energy expenditure, fatty acid oxidation, body temperature, food intake and RER were all preserved between sexes. We similarly observed a potentiated response on food intake in female *ob/ob* mice as in males, indicating that the interaction between leptin and NK2R signalling pathways was independent of sex. We also evaluated NK2R agonism in obese female macaques. The assigned females were ovariectomized in earlier studies unrelated to this research. Although this allowed the maintenance of male–female social housing pairs without the possibility of breeding, the females are more in line with a postmenopausal model. Thus, even though the female macaques responded similarly to males, we could not determine whether there were any interactions between oestrogen and NK2R signalling or how female steroid hormones might affect efficacy in primates.

These findings on dual appetite and energy-expending control by NK2R are particularly surprising given that the tachykinin receptors, NK1R, NK2R and NK3R, are among the oldest known neuropeptide receptor families, with the NK1R ligand substance P even being called the 'pioneering peptide'[54]. Substance P and NK1R have been implicated in metabolic homeostasis through driving food aversion[55], which is in line with the emetic role of NK1R[56]. This is in contrast to our findings that NK2R agonism is non-aversive in mice and that there were no emetic events following any dosing of an NK2R agonist in macaques. NK1R antagonists have even been posited for obesity therapy[57], yet no changes in weight or cardiometabolic parameters were reported after several clinical trials[58]. Exploring the efficacy of NK2R activation has long been impeded by the well-established cross-reactivity of its native ligand NKA with the other tachykinin receptors and the difficulty in generating NK2R-selective molecules that would avoid potential NK1R-linked adverse effects, such as gastrointestinal inflammation, anxiety, bronchoconstriction and pain nociception[5], or NK3R-linked adverse effects, such as hot flushes[59]. Yet decades-old studies in humans comparing infusion of NKA and substance P already hinted at the

potential of NK2R agonism to increase energy dissipation without changes in heart rate[60], but these findings were never expounded upon.

One of the ubiquitous and most pronounced hurdles faced by rodent-based biomedical research and development is translation to humans. We were fortunate to have the opportunity to test the early generation, prototypic NK2R agonist EB1001 in a cohort of older macaques. Every parameter that we were able to measure translated from our observations in rodents to the diabetic, obese macaques, with the added benefit of reduced cholesterol and triglycerides. The recent advances in biopharmaceutical therapies for T2D and obesity have set incredibly high innovation bars[12,13]. However, we believe that features of NK2R agonism such as energy expenditure with no signals of increased cardiovascular risk, lean mass sparing, lack of nausea and, crucially, insulin sensitization could complement the current drug repertoire, particularly in the context of individuals living with both obesity and T2D. Nonetheless, given the translational uncertainty that exists even from nonhuman primate to human pharmacology, the true potential of NK2R agonism and its position and utilization among current cardiometabolic pharmacotherapies will only be realized in clinical trials.

Online content

Any methods, additional references, Nature Portfolio reporting summaries, source data, extended data, supplementary information, acknowledgements, peer review information; details of author contributions and competing interests; and statements of data and code availability are available at https://doi.org/10.1038/s41586-024-08207-0.

1. Christoffersen, B. Ø. et al. Beyond appetite regulation: targeting energy expenditure, fat oxidation, and lean mass preservation for sustainable weight loss. *Obesity* **30**, 841–857 (2022).
2. Müller, T. D., Blüher, M., Tschöp, M. H. & DiMarchi, R. D. Anti-obesity drug discovery: advances and challenges. *Nat. Rev. Drug Discov.* **21**, 201–223 (2022).
3. Coskun, T. et al. LY3437943, a novel triple glucagon, GIP, and GLP-1 receptor agonist for glycemic control and weight loss: from discovery to clinical proof of concept. *Cell Metab.* **34**, 1234–1247.e9 (2022).
4. Finan, B. et al. A rationally designed monomeric peptide triagonist corrects obesity and diabetes in rodents. *Nat. Med.* **21**, 27–36 (2015).
5. Steinhoff, M. S., von Mentzer, B., Geppetti, P., Pothoulakis, C. & Bunnett, N. W. Tachykinins and their receptors: contributions to physiological control and the mechanisms of disease. *Physiol. Rev.* **94**, 265–301 (2014).
6. Maggi, C. A. & Schwartz, T. W. The dual nature of the tachykinin NK1 receptor. *Trends Pharmacol. Sci.* **18**, 351–355 (1997).
7. Drucker, D. J. Mechanisms of action and therapeutic application of glucagon-like peptide-1. *Cell Metab.* **27**, 740–756 (2018).
8. Perdomo, C. M., Cohen, R. V., Sumithran, P., Clément, K. & Frühbeck, G. Contemporary medical, device, and surgical therapies for obesity in adults. *Lancet* **401**, 1116–1130 (2023).
9. Müller, T. D. et al. Glucagon-like peptide 1 (GLP-1). *Mol. Metab.* **30**, 72–130 (2019).
10. Bergmann, N. C., Davies, M. J., Lingvay, I. & Knop, F. K. Semaglutide for the treatment of overweight and obesity: a review. *Diabetes Obes. Metab.* **25**, 18–35 (2023).
11. Lau, D. C. W., Batterham, R. L. & le Roux, C. W. Pharmacological profile of once-weekly injectable semaglutide for chronic weight management. *Expert Rev. Clin. Pharmacol.* **15**, 251–267 (2022).
12. Wilding, J. P. H. et al. Once-weekly semaglutide in adults with overweight or obesity. *N. Engl. J. Med.* **384**, 989–1002 (2021).
13. Jastreboff, A. M. et al. Tirzepatide once weekly for the treatment of obesity. *N. Engl. J. Med.* **387**, 205–216 (2022).
14. Garvey, W. T. et al. Two-year effects of semaglutide in adults with overweight or obesity: the STEP 5 trial. *Nat. Med.* **28**, 2083–2091 (2022).
15. Davies, M. et al. Semaglutide 2.4 mg once a week in adults with overweight or obesity, and type 2 diabetes (STEP 2): a randomised, double-blind, double-dummy, placebo-controlled, phase 3 trial. *Lancet* **397**, 971–984 (2021).
16. Lau, D. C. W. et al. Once-weekly cagrilintide for weight management in people with overweight and obesity: a multicentre, randomised, double-blind, placebo-controlled and active-controlled, dose-finding phase 2 trial. *Lancet* **398**, 2160–2172 (2021).
17. Speakman, J. R. et al. Total daily energy expenditure has declined over the past three decades due to declining basal expenditure, not reduced activity expenditure. *Nat. Metab.* **5**, 579–588 (2023).
18. Cutting, W. C., Mehrtens, H. G. & Tainter, M. L. Actions and uses of dinitrophenol: promising metabolic applications. *J. Am. Med. Assoc.* **101**, 193 (1933).
19. Capozzi, M. E., D'Alessio, D. A. & Campbell, J. E. The past, present, and future physiology and pharmacology of glucagon. *Cell Metab.* **34**, 1654–1674 (2022).
20. Knerr, P. J. et al. Next generation GLP-1/GIP/glucagon triple agonists normalize body weight in obese mice. *Mol. Metab.* **63**, 101533 (2022).
21. Friedrichsen, M. H. et al. Results from three phase 1 trials of NNC9204-1177, a glucagon/GLP-1 receptor co-agonist: Effects on weight loss and safety in adults with overweight or obesity. *Mol. Metab.* **78**, 101801 (2023).

22. Tschöp, M. H. et al. Unimolecular polypharmacy for treatment of diabetes and obesity. *Cell Metab.* **24**, 51–62 (2016).
23. Hauser, A. S., Attwood, M. M., Rask-Andersen, M., Schiöth, H. B. & Gloriam, D. E. Trends in GPCR drug discovery: new agents, targets and indications. *Nat. Rev. Drug Discov.* **16**, 829–842 (2017).
24. Costanzo, M. C. et al. The Type 2 Diabetes Knowledge Portal: An open access genetic resource dedicated to type 2 diabetes and related traits. *Cell Metab.* **35**, 695–710.e6 (2023).
25. Sherwani, S. I., Khan, H. A., Ekhzaimy, A., Masood, A. & Sakharkar, M. K. Significance of HbA1c test in diagnosis and prognosis of diabetic patients. *Biomark. Insights* **11**, 95–104 (2016).
26. Bonnefond, A. et al. Genetic variant in *HK1* is associated with a proanemic state and A1C but not other glycemic control-related traits. *Diabetes* **58**, 2687–2697 (2009).
27. Gjesing, A. P. et al. Studies of a genetic variant in *HK1* in relation to quantitative metabolic traits and to the prevalence of type 2 diabetes. *BMC Med. Genet.* **12**, 99 (2011).
28. Albrechtsen, A. et al. Exome sequencing-driven discovery of coding polymorphisms associated with common metabolic phenotypes. *Diabetologia* **56**, 298–310 (2013).
29. Jurgens, S. J. et al. Analysis of rare genetic variation underlying cardiometabolic diseases and traits among 200,000 individuals in the UK Biobank. *Nat. Genet.* **54**, 240–250 (2022).
30. 1000 Genomes Project Consortium. A global reference for human genetic variation. *Nature* **526**, 68–74 (2015).
31. Yang, Z. et al. CARMA is a new Bayesian model for fine-mapping in genome-wide association meta-analyses. *Nat. Genet.* **55**, 1057–1065 (2023).
32. Moltke, I. et al. A common Greenlandic *TBC1D4* variant confers muscle insulin resistance and type 2 diabetes. *Nature* **512**, 190–193 (2014).
33. Madsen, K. et al. Structure–activity and protraction relationship of long-acting glucagon-like peptide-1 derivatives: importance of fatty acid length, polarity, and bulkiness. *J. Med. Chem.* **50**, 6126–6132 (2007).
34. Chassaing, G. et al. Selective agonists of NK-2 binding sites highly active on rat portal vein (NK-3 bioassay). *Neuropeptides* **19**, 91–95 (1991).
35. Yeo, G. S. H. et al. The melanocortin pathway and energy homeostasis: from discovery to obesity therapy. *Mol. Metab.* **48**, 101206 (2021).
36. Friedman, J. M. Leptin and the endocrine control of energy balance. *Nat. Metab.* **1**, 754–764 (2019).
37. Grill, H. J. & Hayes, M. R. Hindbrain neurons as an essential hub in the neuroanatomically distributed control of energy balance. *Cell Metab.* **16**, 296–309 (2012).
38. Cheng, W. et al. Hindbrain circuits in the control of eating behaviour and energy balance. *Nat. Metab.* **4**, 826–835 (2022).
39. Ludwig, M. Q. et al. A genetic map of the mouse dorsal vagal complex and its role in obesity. *Nat. Metab.* **3**, 530–545 (2021).
40. Hansen, H. H. et al. Whole-brain activation signatures of weight-lowering drugs. *Mol. Metab.* **47**, 101171 (2021).
41. Bingdi Wang, X. W. et al. Dysglycemia and dyslipidemia models in nonhuman primates: part i. model of naturally occurring diabetes. *J. Diabetes Metab.* https://doi.org/10.4172/2155-6156.S13-010 (2015).
42. Inokuchi, T., Watanabe, K., Kameyama, H. & Orita, M. Altered basal C-peptide/insulin molar ratios in obese patients with fatty liver. *Jpn. J. Med.* **27**, 272–276 (1988).
43. Yin, W. et al. Plasma lipid profiling across species for the identification of optimal animal models of human dyslipidemia. *J. Lipid Res.* **53**, 51–65 (2012).
44. Soranzo, N. et al. Common variants at 10 genomic loci influence hemoglobin A_{1C} levels via glycemic and nonglycemic pathways. *Diabetes* **59**, 3229–3239 (2010).
45. Peters, L. L. et al. Downeast anemia (*dea*), a new mouse model of severe nonspherocytic hemolytic anemia caused by hexokinase (HK₁) deficiency. *Blood Cells. Mol. Dis.* **27**, 850–860 (2001).
46. Loos, R. J. F. & Yeo, G. S. H. The genetics of obesity: from discovery to biology. *Nat. Rev. Genet.* **23**, 120–133 (2022).
47. Farooqi, S. & O'Rahilly, S. Genetics of obesity in humans. *Endocr. Rev.* **27**, 710–718 (2006).
48. Jastreboff, A. M. et al. Triple-hormone-receptor agonist retatrutide for obesity—a phase 2 trial. *N. Engl. J. Med.* **389**, 514–526 (2023).
49. Le Roux, C. W. et al. Glucagon and GLP-1 receptor dual agonist survodutide for obesity: a randomised, double-blind, placebo-controlled, dose-finding phase 2 trial. *Lancet Diabetes Endocrinol.* **12**, 162–173 (2024).
50. Palamiuc, L. et al. A tachykinin-like neuroendocrine signalling axis couples central serotonin action and nutrient sensing with peripheral lipid metabolism. *Nat. Commun.* **8**, 14237 (2017).
51. Garfield, A. S. & Heisler, L. K. Pharmacological targeting of the serotonergic system for the treatment of obesity. *J. Physiol.* **587**, 49–60 (2009).
52. Trouwborst, I., Goossens, G. H., Astrup, A., Saris, W. H. M. & Blaak, E. E. Sexual dimorphism in body weight loss, improvements in cardiometabolic risk factors and maintenance of beneficial effects 6 months after a low-calorie diet: results from the randomized controlled DiOGenes trial. *Nutrients* **13**, 1588 (2021).
53. Allegra, S., Chiara, F., Di Grazia, D., Gaspari, M. & De Francia, S. Evaluation of sex differences in preclinical pharmacology research: how far is left to go? *Pharmaceuticals* **16**, 786 (2023).
54. Hökfelt, T., Pernow, B. & Wahren, J. Substance P: a pioneer amongst neuropeptides. *J. Intern. Med.* **249**, 27–40 (2001).
55. Bai, L. et al. Enteroendocrine cell types that drive food reward and aversion. *eLife* **11**, e74964 (2022).
56. Saito, R., Takano, Y. & Kamiya, H.-O. Roles of substance P and NK(1) receptor in the brainstem in the development of emesis. *J. Pharmacol. Sci.* **91**, 87–94 (2003).
57. Karagiannides, I. et al. Substance P as a novel anti-obesity target. *Gastroenterology* **134**, 747–755 (2008).
58. Quartara, L., Altamura, M., Evangelista, S. & Maggi, C. A. Tachykinin receptor antagonists in clinical trials. *Expert Opin. Investig. Drugs* **18**, 1843–1864 (2009).
59. Mullard, A. FDA approves first-in-class NK3 receptor antagonist for hot flushes. *Nat. Rev. Drug Discov.* **22**, 526 (2023).
60. Evans, T., Dixon, C., Clarke, B., Conradson, T. & Barnes, P. Comparison of neurokinin A and substance P on cardiovascular and airway function in man. *Br. J. Clin. Pharmacol.* **25**, 273–275 (1988).
61. Nédélec, Y. et al. Genetic ancestry and natural selection drive population differences in immune responses to pathogens. *Cell* **167**, 657–669.e21 (2016).
62. Quach, H. et al. Genetic adaptation and Neandertal admixture shaped the immune system of human population. *Cell* **167**, 643–656.e17 (2016).

Methods

Mice

Mouse studies performed at the University of Copenhagen were approved by The Danish Animal Experiments Inspectorate (permit number: 2018-15-0201-01441 and 2023-15-0201-01386) and the University of Copenhagen. Animal experiments performed at the University of Michigan were approved by the University of Michigan Committee on the Use and Care of Animals (protocol no. 00011066) and in accordance with Association for the Assessment and Approval of Laboratory Animal Care and National Institutes of Health guidelines. Studies in Fig. 1p–r using EB0014 were conducted by Gubra. Mice were housed in solid bottom cages with environmental enrichment at 22 °C (±2 °C) in 55% (±10%) humidity and a 12-h light:dark cycle (light from 06:00 to 18:00). Mice had ad libitum access to water and standard chow diet (SAFE D30, Safe Diets) or 60% HFD (Rodent Diet with 60 kcal% fat, D12492i, Research Diets) to induce obesity as indicated in the figure captions and results. For studies with DIO mice, mice were challenged with HFD for a minimum of 12 weeks starting from 8 weeks of age and were used in pharmacology studies once the mean cohort size was at least 35 g. Groups were randomized for vehicle and compound treatment. Pharmacological DIO studies in wild-type male and female mice were performed on animals with a C57Bl/6 NRj genetic background (Janvier Labs). The description of backgrounds for the genetic models used are as follows: B6.V-*Lep^ob*/JRj (*ob/ob*) mice and RjOrl:SWISS (CD-1) mice were purchased from Janvier Labs. B6.129S4-*Mc4r^tm1Lowl*/J (*Mc4r*-knockout), *Cck^tm1.1(cre)Zjh*/J, B6.129-*Lepr^tm3(cre)Mgmj*/J, *Calcr^tm1.1(cre)Mgmj*/J, B6;129-*Gt(ROSA)26Sor^tm5(CAG-Sun1/sfGFP)Nat*/J and Gt(ROSA)26Sor^tm1(CAG-EGFP/Rpl10)Dolsn mice were purchased from the Jackson Laboratory. The *Ucp1*-knockout line was provided by K. Kristiansen. B6N-Tacr2^tm1Zpg (*Nk2r*-floxed) mice were generated by GenOway on a C57Bl/6N background by inserting *lox*P sites around exon 1, which encodes 130 out of the 384 amino acids in the full-length receptor. *Ucp1*-knockout, *Nk2r*-knockout and *Nk2r*-floxed lines were bred in-house at 22 °C (± 2 °C). *Cck^tm1.1(cre)Zjh*/J and B6.129-*Lepr^tm3(cre)Mgmj*/J mice were crossed with Gt(ROSA)26Sor^tm1(CAG-EGFP/Rpl10)Dolsn mice to create *Cck*^Cre L10 GFP and *Lepr*^Cre L10 GFP mice respectively. *Calcr^tm1.1(cre)Mgmj*/J mice were crossed with B6;129-*Gt(ROSA)26Sor^tm5(CAG-Sun1/sfGFP)Nat*/J to create *Calcr*^Cre Sun1 GFP mice. Studies were generally performed at 22 °C (±2 °C). Studies in *Ucp1*-knockout mice and the *ob/ob* one time injection and subcutaneous/ICV crossover study were performed in thermoneutrally (29 °C (±2 °C)) housed mice.

Mice were trained with mock injections for all injection studies for at least 5 days. NKA (1 mg kg⁻¹; Almac) dissolved in Gelofusine (B. Braun) was administered subcutaneously twice daily for 9 consecutive days. EB0014 (synthesized by Almac) was dissolved in DMSO to a 17 mg ml⁻¹ solution and further in 0.9% saline with 3% BSA. EB0014 was subcutaneously administered once daily at 1 mg kg⁻¹ for indirect calorimetry measurements and at 0.01 mg kg⁻¹, 0.1 mg kg⁻¹, 0.3 mg kg⁻¹ and 1 mg kg⁻¹ for the dose-dependent weight loss study.

EB1002 (synthesized by Novo Nordisk or PolyPeptide) was dissolved in 8 mM phosphate and 240 mM propylene glycol (pH 8.2) and administered once, daily for 7 or 21 consecutive days or every other day for 21 days via subcutaneous injections at 40 nmol kg⁻¹ or 325 nmol kg⁻¹ between 15:00 and 16:00. The NK2R antagonist, saredutant (SR 48968, MedChemExpress), was injected into the peritoneum at 5 mg kg⁻¹ in 0.9% saline with 1% Tween80 30 min prior to EB1002 injections. Body weight, blood glucose and food weight were taken immediately before injections and 24 h after injections. The amount of food for pair-fed groups was determined on the basis of at least two previous studies. To mimic a diet intervention, DIO mice were switched to chow diet 5 days prior to first injection and compared to DIO mice maintained on HFD. The effect of EB1002 on food intake in Extended Data Fig. 5a was assessed in overnight-fasted mice that were refed at the time of injection.

The insulin tolerance test was performed in DIO mice after the 9-day injection regimen, 12 h after the final injection with 1 mg kg⁻¹ NKA. Insulin tolerance test was carried out on 4-h fasted mice by intraperitoneal injection of 0.75 U kg⁻¹ insulin. Twenty-four hours prior to the glucose tolerance test, DIO mice were subcutaneously injected with vehicle or 325 nmol kg⁻¹ EB1002. Vehicle-treated mice had either ad libitum access to HFD or were pair-fed to EB1002-treated mice. Glucose tolerance test was performed the following day on 4-h fasted mice by intraperitoneal injection of 1 g kg⁻¹ glucose. Insulin levels were measured using the Mouse/Rat Insulin Kit (mesoscale) according to the manufacturer's protocol.

GLP-1, leptin, glucagon and PYY were measured in plasma samples using the U-PLEX Gut Hormone Combo 1 (ms) SECTOR Kit (MSD, K15307K-1) according to the manufacturer's protocol.

To evaluate the aversive potential in mice, a saccharin-conditioned taste avoidance was performed as described[63]. On the conditioning day, mice were exposed to a new flavour (0.15% saccharin) followed by a subcutaneous injection of vehicle, 10 nmol kg⁻¹ semaglutide or 325 nmol kg⁻¹ EB1002.

Liquid phase gastric emptying was performed in 4-h fasted mice. Mice received an injection of vehicle or EB1002 30 min prior to an oral gavage of 4 mg paracetamol in 0.9% NaCl. Blood samples were collected via the tail vein 15 min after gavage and paracetamol levels were measured using Acetaminophen L3K assay kit (Sekisui Diagnostics, 506-30) according to the manufacturer's protocol.

Tissue-specific insulin signalling was assessed in mice 18 h after injection with vehicle or EB1002. 2 h fasted mice were sedated with 75 mg kg⁻¹ pentobarbital (intraperitoneal injection) and received a retro orbital injection with 1.5 U kg⁻¹ insulin. Tissues were dissected 10 min after insulin administration, snap-frozen and analysed as described in 'Immunoblotting'.

Total lean and fat mass were measured by magnetic resonance imaging using the minispec LF90 II body composition analyser (Bruker).

Metabolic characterization

Oxygen consumption, carbon dioxide production and food intake were recorded using the Promethion core system (Sable Systems International) with data processing using OneClickMacroV2.52.1 and Macrointerpretersetup_v2_47 or the Phenomaster Home Cage System (TSE Systems) with PhenoMaster software v.8.2.9. Generally, mice were transferred to training cages 3–7 days prior to the measurement and were allowed to acclimate in the measurement chambers for at least 24 h or until a stable baseline was observed. Fatty acid oxidation was calculated using the formula[64]: energy expenditure (kcal/h) × (1-RER)/0.3.

Core body temperature and gross motor activity measurements

Continuous body temperature and motor activity were measured with G2 E-Mitter telemetric devices (Starr Life Sciences) or with radio frequency identification (RFID) temperature transponders (UCT-2112 microchips, Unified Information Devices). Probes were implanted into the peritoneal cavity under sterile conditions. In brief, mice were anaesthetized with isoflurane and received 5 mg kg⁻¹ Rimadyl (ScanVet, 027693) and 8 mg kg⁻¹ Lidocaine (AstraZeneca). The sterile probe was inserted into the peritoneum via a midline incision. After closure, mice were allowed to recover on a heated surface and received 5 mg kg⁻¹ Rimadyl for 3 consecutive days. Mice were allowed to recover for at least 7 days before study start. E-mitter data was recorded by placing ER4000 Receivers under the cages within the TSE cabinet. Temperature data was integrated in the Phenomaster software. RFID temperature transponder data was recorded by using UID Mouse Matrix system (Unified Information Devices) in combination with the Sable system.

Article

Triple-chip study

RFID temperature transponders (UCT-2112 microchips, Unified Information Devices) were surgically implanted and anchored in female mice for continuous and simultaneous measurement of temperature in three distinct anatomical locations. Surgical and post-operative procedures were performed as described above. Ventromedial abdominal chip (abdominal temperature): following a midline incision, the chip was inserted in the abdominal cavity. Distolateral femoral chip (hindlimb temperature): following a transverse left gluteal incision, a subcutaneous lateral femoral pocket was prepared, and the chip was inserted. Dorsomedial intrascapular chip (interscapular temperature) and bilateral BAT denervation: following a midline dorsal incision, the interscapular BAT was detached from the underlying muscle layer. Bilateral denervation was performed as described[65]. The chip was inserted with the tip containing the temperature probe placed between the BAT and the dorsal muscle. The three temperatures were recorded using the UID Mouse Matrix system (Unified Information Devices).

Brain cannulation and ICV injections

For administration of compounds directly into the brain of awake mice, a cannula was placed into the cerebral ventricle. B6.V-Lep^{ob}/JRj (*ob/ob*) mice were anaesthetized with isoflurane and received 5 mg kg^{-1} Rimadyl (ScanVet, 027693) and 8 mg kg^{-1} Lidocaine (AstraZeneca). Mice were fixated in a stereotaxic frame (Kopf Instruments) and the scalp was opened to expose the skull. Coordinates were zeroed on bregma and moved to −0.3 mm in the anteroposterior axis and −1.0 mm in the mediolateral axis. A small hole was drilled into the skull and the guide cannula (C315GS-4/Spc 2 mm, PlasticsOne) was inserted and fixated using a G-bond layer (GC America) and G-ænial universal flow (GC America). Finally, a dummy (C315DCS-4/Spc 2.5 mm, PlasticsOne) was screwed onto the guide cannula and mice were allowed to recover on a heated surface and received 5 mg kg^{-1} Rimadyl for 2 consecutive days following the surgery. To test the correct placement of the cannula, mice received an infusion of 1.5 µl of 24 µM angiotensin II (Sigma) in artificial cerebrospinal fluid (CSF) (Harvard Apparatus) via an injector (C315IS-4/Spc 2.5 mm, PlasticsOne) and an infusion pump (Harvard Apparatus) at a rate of 2 µl min^{-1} 5 days after surgery. After the infusion, the injector was left in place for an additional 45 s to minimize backflow. Then, the injector was removed, and the dummy was placed on the cannula. Mice were monitored for angiotensin II-induced water intake and responsive mice were subsequently used for ICV injection studies. One week prior to study start, mice were housed at thermoneutrality. Mice first received a single subcutaneous injection of vehicle or 325 nmol kg^{-1} EB1002 and after a wash-out period they were infused with 1.5 µl artificial CSF or 2 nmol EB1002 in 1.5 µl artificial CSF as described above in a crossover design.

AAV injections into the DVC of *Nkr2*-floxed mice

Nk2r$^{fl/fl}$ mice were anaesthetized using isoflurane. Mouse heads were oriented at a 90° angle and an incision was made at the caudal aspect of the skull to expose the brainstem. Using the obex of the skull as a guide, 50 nl of AAV-GFP or AAV-CMV-CRE-GFP were injected into each site of the DVC at a depth (*z*) of 0.350 mm. Virus was injected at a rate of 15–35 nl min^{-1}. The pipette remained in the DVC for an additional 3 min to allow viral particles to disperse, and then the pipette was slowly removed. Mice received prophylactic analgesic carprofen (5 mg kg^{-1}) before and for 24 h after surgery and were monitored for 10 days following the procedure to ensure recovery for surgical intervention. Mice were fed a 60% HFD starting 6 weeks after surgery for 5 weeks. To assess the acute food intake response to EB1002, mice were injected subcutaneously with either vehicle or 325 nmol kg^{-1} EB1002 in a crossover design. Food intake was measured at hours 0, 1, 2, 4 and 24 and body weights were recorded at 0 and 24 h post-injection. After termination, hit sites of all mice were confirmed using immunohistochemistry and mice with a confirmed bilateral hit site were included in the analysis.

Hyperinsulinaemic–euglycaemic clamp and peripheral glucose uptake

Hyperinsulinaemic–euglycaemic clamps were performed in conscious, unrestrained male mice at 24 weeks of age as previously described[66]. In short, catheters were implanted under aseptic conditions into the right jugular vein (C20PU-MJV1458; Instech) and the left common carotid artery (C10PU-MCA1459; Instech), exteriorized in the scapular region and secured using a dual-channel vascular access button (VABM2B/25R25; Instech) under general isoflurane anaesthesia. Mice were subcutaneously injected preoperatively with Carprofen (5 mg kg^{-1}, Norodyl Vet, Scanvet) for analgesia and a mixture of Lidocaine (7 mg kg^{-1}, Xylocain, AstraZeneca) and Bupivacaine (7 mg kg^{-1}, Marcaine, Orifarm) at the incision sites for local anaesthesia. Mice were allowed to recover for 7–10 days. Mice were treated with either vehicle or 325 nmol kg^{-1} EB1002 24 h prior to clamp experiment. Clamp studies were performed in 4 h fasted mice. At 15 min and 5 min before the start of the clamp, blood samples were taken for determination of basal glucose and insulin levels. At 0 min, the clamp was initiated with continuous infusion of human insulin (4mU kg^{-1} min^{-1}, Actrapid; Novo Nordisk, Denmark). Donor red blood cells were washed and used to compensate for the blood loss to experimental mice during the repeated sampling (5 µl min^{-1} of 50% RBC in 10 U ml^{-1} heparinized saline). Blood glucose samples were taken every 10 min (Contour XT, Bayer) and blood glucose was then adjusted using a variable infusion of 50% glucose. Both human and mouse insulin levels (Mercodia) were determined at 100 and 120 min. After 120 min, a 13 µCi bolus of 2-[1-^{14}C]-deoxy-D-glucose was given and blood samples taken at 122, 125, 135, 145 and 155 min and specific activity for 2-[1-^{14}C]-deoxy-D-glucose was determined in these samples. After euthanization, tissues for tissue-specific 2-[1-^{14}C]-deoxy-D-glucose uptake were sampled and snap-frozen in liquid nitrogen. Samples from tissue-specific glucose uptake were processed as previously described[66].

Pharmacological pre-toxicology evaluation

For the evaluation of potential toxicological effects CD-1 outbred mice were daily either injected with vehicle or with increasing concentrations of EB1002 (150 nmol kg^{-1} (2 consecutive days), 300 nmol kg^{-1} (2 consecutive days), 600 nmol kg^{-1} (2 consecutive days), 1,200 nmol kg^{-1} (2 consecutive days), 2,400 nmol kg^{-1} (2 consecutive days), 4,800 nmol kg^{-1} (2 consecutive days) and finally 7,500 nmol kg^{-1} (3 consecutive days)). Liver, spleen, heart, kidney, oesophagus, stomach, duodenum, colon, testis, cornea, bladder and thymus were dissected, fixed in 10% formalin and stained with haematoxylin and eosin for pathohistological analysis performed by the Histology department, HistoCore, at the University of Copenhagen. Slides were compared pairwise. Serum liver enzymes were analysed by the Veterinary Diagnostic Laboratory core at the University of Copenhagen.

Quantification of faecal cholesterol and triacylglycerides

Faecal samples were homogenized in cold methanol containing butylated hydroxytoluene (1 mg ml^{-1}). After centrifugation (10 min at 10,000g, 4 °C), the supernatants were transferred into fresh vials and the methanol was evaporated by vacuum centrifugation. Pellets were re-dissolved in 0.1 M potassium phosphate, pH 7.4, 0.05 M NaCl, 5 mM cholic acid and 0.1% Triton X-100. Cholesterol and triacylglycerides were quantified using colorimetric kits from DiaSys (Cholesterol (113009910704) and triacylglycerides (157109910026)) according to the manufacturer's instructions.

NKA and compound detection in the blood

Pharmacokinetic profiles were determined in lean mice. Mice were subcutaneously dosed with 1 mg kg^{-1} NKA, 666.3 nmol kg^{-1} EB0014, 325 nmol kg^{-1} EB1001 and 325 nmol kg^{-1} EB1002. Blood samples were taken starting at 5 min until 60 h as indicated in respective graphs. Plasma levels of NKA were determined using a Human Neurokinin A kit Elisa Kit (Ray Biotech). Plasma levels of EB0014, EB1001 and EB1002

were determined using LC-MS after precipitation with acetonitrile containing 0.1% formic acid.

In situ hybridization

Wild-type mice were anaesthetized with 75 mg kg^{-1} pentobarbital and transcardially perfused with 4% paraformaldehyde (PFA) in PBS. Whole brains were dissected, further fixated in 4% PFA in PBS for 48 h at 4 °C and subsequently dehydrated using the automated Excelsior AS tissue processor (Thermo Scientific) and embedded in paraffin. Paraffin-embedded brains were cut into 4 μm sections using the Microm Ergostar HM 200 (Marshall Scientific) and mounted onto glass slides. After deparaffination and rehydration, RNA molecules were detected using the RNAscope Multiplex Fluorescent V2 Assay kit (ACDbio) according to manufacturer's protocol. *Nk2r*, *Calcr* and *Glp1r* were detected with the RNAscope probes Mm-Tacr2 (441311), Mm-Calcr-C2 (494071-C2) and Mm-Glp1r-C3 (418851-C3), and 3-plex Negative probe (320871) and 3-plex-mouse Positive probe (320881, all ACDbio) were used as negative and positive control respectively. Signals were visualized with fluorophores at 570 nm (OP-001003) for channel 1, 520 nm (OP-001006) for channel 2 and 690 for channel 3 (OP-001001, all 1:1000, Akoya Bioscience). Sections were mounted with ProLong Gold antifade reagent with DAPI (P36935, Invitrogen). For analysis, 4 mice were used and 2–3 sections per animal were imaged.

Immunohistochemistry

Mice were fasted overnight and injected subcutaneously with vehicle or 325 nmol kg^{-1} 2 h prior to euthanasia. Mice anaesthetized with isoflurane and transcardially perfused with PBS followed by 4% PFA in PBS. Whole brains were dissected, further fixated in 4% PFA in PBS for 4 h at 22 °C. After 48 h in a 30% sucrose solution, brains were cut into 30 μm sections using a sliding microtome SM2010R (Leica) with a freezing stage and temperature controller (BFS40-MPA, Physiotemp). Free floating sections were blocked in 3% donkey serum with 0.1% Triton X-100 in PBS and incubated overnight at room temperature using the following antibodies, against FOS (Cell Signalling, 2250, 1:1,000) and GFP (Aves Laboratories, 1020, 1:1,000). Sections were washed, incubated with a secondary antibody conjugated to Alexa Fluor 488 and 568 (Invitrogen, A-11039, A-11011, 1:250) and mounted.

To assess neuronal degradation in the DVC of *Nk2r*$^{DVC-GFP}$ and *Nk2r*$^{DVC-cre}$ mice, the Fluoro-Jade C (FJC), RTD Ready-to-Dilute Staining Kit for identifying Degenerating Neurons (VWR) was applied according to manufacturer's instructions. Fluoro-Jade C positive neurons were counted for quantification of neuronal degradation.

Microscopy

Fluorescence microscopy was performed using a Zeiss Axio Observer microscope with Axiocam 702 mono camera or with an Olympus BX53 microscope.

Whole-brain FOS imaging

Two-hour fasted obese wild-type mice received a single subcutaneous dose of vehicle or 325 nmol kg^{-1} EB1002 before being terminated and perfused with 4% PFA 2 h later. The brains were subsequently isolated, postfixed, and transferred to Gubra. At Gubra, the samples were cleared, stained for FOS, and imaged at single-cell resolution using a light sheet microscope as previously described[40]. The data from individual brains was mapped into an average mouse brain atlas template, and the number of FOS labelled cells was quantified in more than 800 brain regions. For the calculation of fold changes, brain regions without FOS signal ($n = 25$) were excluded.

Immunoblotting

Protein was isolated and western blots were run as described previously[67]. Proteins were detected using the following antibodies, AKT (Cell Signaling, 9272, 1:1,000), pAKT T308 (Cell Signalling, 9275,

1:1,000), Tyrosine hydroxylase (Abcam, ab137869, 1:1,000), UCP1 (Abcam, ab10983, 1:7,500) and peroxidase-conjugated AffiniPure Goat Anti-Rabbit IgG (H+L) (Jackson Immuno Research, 111-035-144, 1:5,000). Images were acquired using an Odyssey Fc Imager (LI-COR). Uncropped images can be found in the source data.

snRNA-seq

Mice were injected subcutaneously with vehicle or 325 nmol kg^{-1} EB1002 2 h prior to euthanasia. After decapitation, the brain was removed, and the DVCs were isolated from the brainstem under a surgical microscope. A 1 mm coronal section of the hindbrain from bregma −7.0 to −8.0 mm was cut with a razor blade. From the coronal section, a 1.4 mm square containing the DVC was snap-frozen. Samples from the same experimental condition were pooled ($n = 5$ mice per sample). Nuclei were extracted as previously described[68]. Sorting of 2n nuclei was performed by flow cytometry using a BD FACSAria IIIu Influx cell sorter (BD Biosciences). The gating was set according to size and granularity using FSC and SSC to capture singlets and remove debris. To detect DraQ5-positive nuclei fluorescence was set at 647 nm and 670 nm. Each sample was sorted into separate tubes, each with a total of 20,000 nuclei per 40 μl. Sequencing libraries were generated using 10x Genomics Chromium Single-Cell 3′ Reagent kit according to the standardized protocol. Paired-end sequencing was performed using an Illumina NovaSeq 6000.

snRNA-seq analysis. Raw sequencing data were demultiplexed, aligned to the mouse reference genome GRCm38 (mm10) and counted using cellranger (version 7.0.0; 10x Genomics). Ambient RNA molecules were removed from cellranger raw count matrix files with cellbender:remove-background (v0.3)[69]. Filtered count matrices were analysed in R with Seurat (v4.3.0)[70]. Nuclei with at least 1000 detectable genes were retained. Genes expressed in at least 10 nuclei were retained. ScDblFinder (v1.15.4)[71] with standard parameters was run on individual 10x lanes to remove doublets. The count data were normalized with NormalizeData and scaled with ScaleData function. Genes were then defined as variable using FindVariableFeatures and used as input into principal components analysis with RunPCA. The top 30 principal components were retained and used for further dimensionality reduction using RunUMAP and clustered using a resolution of 0.8 with FindClusters. To perform cell-type-specific quality control, the nuclei were split into two broad categories, neuronal and nonneuronal, using CellAnnotatorR(v), on the basis of the expression of neuronal marker gene *Rbfox3* or *Snap25* and the absence of nonneuronal markers. Neuronal data was further filtered by removing nuclei with unique molecular identifiers (UMIs) in the first and 99th percentile. Library complexity was calculated by dividing the log of the total genes detected per nuclei by the log of the total UMIs per nuclei. Nuclei in the first percentile of this metric were removed. Add_Mito_Ribo_Seurat was used to identify and remove nuclei with >1% mitochondria and ribosomal genes. We finally removed outliers by isOutlier with nmads = 5 run on individual 10x lanes from the package SingleCellExperiment[72]. After all quality control, a total of 23,664 neurons remained. Neuronal cell types were labelled by projecting labels from a previously published dataset[39] (GSE166649) using Seurat FindtransferAnchors and TransferData function.

Immediate early gene analysis. To calculate an IEG score, rapid primary response genes[73] (*Fosb*, *Npas4*, *Fos*, *Junb*, *Nr4a1*, *Arc*, *Egr2*, *Egr1*, *Maff*, *Ier2*, *Klf4*, *Dusp1*, *Gadd45g*, *Dusp5*, *Btg2*, *Ppp1r15a* and *Amigo3*) were used to score each nuclei with the AddModuleScore function from Seurat. For each cluster-sample combination we calculated the average activity score which we then modelled by the interaction of cell type and treatment. Estimated marginal means were compared between treatments within each cluster. *P* values were corrected for multiple testing using the Benjamini–Hochberg method (adjusting for the number of cell populations).

Article

Perturbed cell-type analysis. We used the scDist package to calculate the transcriptional distance between treatment and controls while also controlling for individual-to-individual variability[74].

Primary cell studies

Primary white adipocytes were isolated for wild-type mice and cultures as described[75]. For in vitro oxygen consumption measurements, cells were replated in Seahorse XF96 Cell Culture Microplates (Agilent Technologies) on day 3 and oxygen consumption in response to vehicle or EB1002 (10 nM, 1 μM and 10 μM) was measured using a Seahorse XFe96 Extracellular Flux Analyzer (Agilent Technologies) on day 7 as described[75]. For in vitro glucose uptake, differentiated cells were starved for 2 h before treatment with Krebs-Ringer buffer containing 5 mM glucose, and vehicle or EB1002 (10 nM, 1 μM and 10 μM). After 2 h, cell media was incubated with a reaction mix mix (200 mM Tris-HCl, 500 mM $MgCl_2$, 5.2 mM ATP, 2.8 mM NADP, and 6 μg ml^{-1} hexokinase and glucose-6-phosphate dehydrogenase mixture (10737275001, Roche Diagnostics)) for 15 min and glucose content was measured spectrophotometrically at 340 nm (Hidex sense, Hidex). Glucose uptake was calculated on the basis of disappearance of glucose from the media. Cells have been tested negative for mycoplasma contamination.

Ex vivo lipolysis

To assess the effects of EB1002 on the lipolytic function of adipocytes, mature adipocytes were isolated from iWAT of wild-type chow-fed mice. In brief, adipose depots were minced and digested in Krebs-Ringer buffer containing 2% BSA and 0.2% collagenase type I (Worthington Biochemical) at 37 °C. Cells were passed through a 100-μm cell strainer, centrifuged (10 min, 10g, 4 °C) and the floating mature adipocyte fraction was washed three times. Cells were incubated with vehicle, EB1002 (10 nM, 1 μM and 10 μM) or 50 nM isoproterenol for 2 h at 37 °C. Finally, non-esterified free fatty acids were measured in the medium using the Fujifilm NEFA HR R2 kit according to manufacturer's protocol.

Macaque studies

The macaque studies were conducted in compliance with all federal regulations, including the US Animal Welfare Act. Studies were reviewed and approved by the OHSU/ONPRC Institutional Animal Care and Use Committee. The ONPRC is accredited by AAALAC International. For these studies, 10 rhesus macaques (5 males and 5 ovariectomized females, 12–23 years of age with a body weight ranging from 7–24 kg) were pair-housed (1 male and 1 female) in custom designed cages (Carter2 Systems) in shared rooms under fixed photoperiodic conditions (lights on from 07:00 to 19:00). The cages meet the minimum European Union accepted standards for housing nonhuman primates (2.0 m^2 enclosure size, 3.6 m^3 enclosure volume, and 1.8 m enclosure height). Shelves, verandas, solid flooring and changeable plastic toys were available for the monkeys. The commercially available HFD (5L0P, Lab/Test Diets) was provided ad libitum twice every day. Food intake was measured daily, and animals were separated for 1–2 h periods when individual food intake was measured. Paired food intake was measured for the remaining feeding times when animals were socially pair-housed.

EB1001 was dissolved in 8 mM phosphate and 240 mM propylene glycol (pH 8.2) and administered for 8 consecutive weeks via subcutaneous injections between 08:00 and 09:00 prior to the morning meal. All animals were started on the 30 nmol kg^{-1} dose with every other day dosing (q48h) for 1 week, followed by daily dosing of the subsequent higher doses. Dose escalations were as follows (nmol kg^{-1}): 60 (1 week), 90 (1 week), 120 (1 week), 240 (2 weeks), 480 (4 days) and 240 (10 days). Body weight was measured on a weekly basis using the same, calibrated digital scale. Heart rate and oxygen saturation were recorded in sedated animals using a pulse oximeter (Model 7500, Nonin Medical).

Blood samples were collected in conscious animals prior to morning meal (overnight fast) and daily dose administration. Blood glucose was measured on a Biosen clinical analyser (EKF Diagnostics) and C-peptide and insulin were measured on a Cobas e411 analyser (Roche Diagnostics). Remaining chemistry parameters alanine aminotransferase (ALT), aspartate transaminase (AST), total cholesterol (Chol), creatinine (CREA), glucose triglyceride (TG), blood urea nitrogen (BUN) and LDL cholesterol were analysed using the Pentra C400 (Horiba Medical).

Behaviour analysis was performed by members of the ONPRC Behavioural Sciences Unit blinded to the experimental design. Observations were taken directly on a mobile device and average behaviour scores were calculated on the basis of events such as anxiety, stereotypy, eye poking or withdrawn behaviour. Additional cage side observations included signs of nausea (gaping and hunched posture), emesis and stool consistency.

Association of missense variants with cardiometabolic traits

To assess whether the 4 missense NK2R variants (R3232H, I23T, V54I and A161T) are associated with cardiometabolic traits, their associations in T2D Knowledge Portal (HbA1c phenotype page, accessed 21 May 2024; https://t2d.hugeamp.org/phenotype.html?phenotype=HBA1C; RRID:SCR_003743)[24] were queried. For each variant, only the associations that presented a P value < 0.05 for the latest and largest European genome-wide association study (GWAS) per trait were included. Additionally, the minor allele frequency in five ancestries are reported: AFR, AMR, EAS, EUR and SAS retrieved from 1000 Genomes reference panel data from dbSNP[30,76].

SNP-level associations in the *HK1*–*NK2R*–*TSPAN15* region

Utilizing the latest and largest European GWAS of HbA1c available in T2D Knowledge Portal (query on 10/05/2024) (HbA1c phenotype page, accessed 21 May 2024; https://t2d.hugeamp.org/phenotype.html?phenotype=HBA1C (RRID:SCR_003743))[24], summary statistics from Jurgens et al.[29] were retrieved and 1,944 common variants (minor allele frequency > 1%) located 100 kilobases (kb) upstream from the *HK1* transcription start site (TSS) and 100 kb downstream from the *TSPAN15* TSS (10:70929740–71367422) were investigated further.

The number of lead, independent, genome-wide significant variants were assessed by performing LD clumping with with plink1.9 (ref. 77) and utilizing the European 1000 Genomes reference panel phase 3 version 5 (ref. 30). An r^2 threshold of 0.01 and distance threshold of 1,000 kilobases (kb) were used.

Fine mapping of HbA1c associations in 10:70929740–71367422 locus with CARMA[31], a software designed to correct for differences in LD between summary statistics and LD reference panels were performed. CARMA with the default settings, utilizing European 1000 Genomes reference panel phase 3 version 5 with annotations[30] were performed, and those variants that presented a posterior inclusion probability of >0.1 were investigated further. In dbSNP[76], minor allele frequencies in five genetic ancestries were retrieved: AFR, AMR, EAS, EUR and SAS.

Finally, Open Target Genetics (OTG)[78] was utilized to query the variant-to-gene (V2G) scores used for gene prioritization and the associations of causal variants with eQTLs.

Linkage disequilibrium analysis

All analyses were performed in Rstudio (2022.07.2 + 576) with R (4.1.3). Data were loaded and manipulated using data.table (1.14.2) and tidyverse (1.3.1). LD operations were performed using plink1.9 (ref. 77), ggLD (https://github.com/mmkim1210/ggLD), and LDLink[79]. All results can be reproduced by following the code available at https://github.com/MarioGuCBMR/nk2r_hk1_genetics.

TWAS of *NK2R* and HbA1c

Elastic Net model of SPrediXcan methods were used to predict the association between gene and traits[80–82]. The Elastic Net-based GTEx v8 eQTL models were downloaded from https://predictdb.org/post/2021/07/21/gtex-v8-models-on-eqtl-and-sqtl/. The summary statistics of GWAS for

BMI[83], HbA1c levels (total sample based)[83], and BMI-adjusted HbA1c levels (total sample based)[84] were used to conduct the association analysis. The SNPlocs.Hsapiens.dbSNP144.GRCh37 Bioconductor package[85] was used to convert the genomic coordinates of SNPs to rsID for the summary statistics of HbA1c and BMI-adjusted HbA1c. Sensitivity analysis was performed using the CAVIAR fine-mapped variants[86] for NK2R in nucleus accumbens of the brain tissue.

Genetic association studies in Greenlanders
Blood samples from Greenlanders collected in three population surveys (data are available at ref. 87 and https://www.sdu.dk/da/sif/rapporter/2011/inuit_health_in_transition and https://www.sdu.dk/da/sif/rapporter/2019/befolkningsundersoegelsen_i_groenland) were genotyped using the Multi-Ethnic Global Array (Illumina). After quality control up to 5,758 individuals were available for association analyses. Metabolic phenotypes were measured as previously described[88], and association analyses were performed with a linear mixed model, to account for relatedness and admixture, assuming an additive genetic model and adjusting for age, sex, cohort using GEMMA[89]. We performed association tests for all 132 variants within the coding region of *NK2R* and the 3′ and 5′ untranslated regions ±1,000 bp. The strongest associations across traits related to body composition were observed for the non-coding rs139900276 variant. RNA was extracted from peripheral blood for a subset of 499 individuals. The procedure for RNA extraction, sequencing, quality control, and quantification has previously been described[88]. *NK2R* expression according to rs139900276 genotype was tested with a linear mixed model adjusted for sex, age, and top ten principal components from a principal components analysis of the normalized expression matrix.

Mutation of human wild-type *NK2R*
SNPs identified by GWAS were introduced to human wild-type *NK2R* coding sequence (NP_001048.2) in a custom pCDNA3.1(+) vector (Genscript) using PCR-based QuickChange Site-Directed Mutagenesis (Agilent) according to manufacturer's protocol. Mutated vector was introduced to *Escherichia coli* to amplify DNA and indicated mutations were confirmed by forward and reverse strand Sanger sequencing (Eurofins). PCR primers used to introduce mutations are as follows (forward, reverse): I23T (CAACACCACGGGCACG ACAGCCTTCTCCA, TGGAGAAGGCTGTCGTGCCCGTGGTGTTG), V54I (TGACGGGTAATGCCATCATCATCTGGATCATCCTG, CAGGA TGATCCAGATGATGGCATTACCCGTCA), A161T (CTGGTGGCTCTC ACCCTGGCCTCCC, GGGAGGCCAGGGTGAGAGCCACCAG), R323H (CCGGCTTGCCTTCCATTGCTGCCCATGG, CCCATGGGCAGCAATGGA AGGCAAGCCGG), T346M (CGACCTCCCTCTCCATGAGAGTCAAC AGGTG, CACCTGTTGACTCTCATGGAGAGGGAGGTCG), T363A (TGGCTGGGGACGCAGCCCCCTCC, GGAGGGGGCTGCGTCCCC AGCCA), H395R (TTGCCCCCACCAAAACTCGTGTTGAAATTTGAGGATC, GATCCTCAAATTTCAACACGAGTTTTGGTGGGGGCAA).

Receptor activity assays
NKA-induced activation of mutated human NK2R and substance P-, NKA-, NKB-, EB1001- and EB1002-induced activation of mouse and human wild-type NK1R, NK2R and NK3R were measured by inositol-1,4,5-trisphosphate [³H] Radioreceptor assay (IP₃ assay). IP₃ assays were carried out using COS-7 cells (ATCC, CRL-1651) transiently transfected by calcium phosphate transfection with one of the mutated NK2R variants or the wild-type receptors as previously described[75]. The IP₃ assay was performed the day after transfection. In brief, cells were washed and pre-incubated in assay buffer (HBSS, 10 mM LiCl, 0.2% w/v ovalbumin) for 30 min followed by 120 min incubation with substance P, NKA, NKB, EB1001 or EB1002 at 37 °C as indicated in result section and figure legends. After incubation, plates were immediately placed on ice, and cells were lysed (10 mM formic acid). After 30 min incubation 1 mg per well SPA YSI beads were pipetted into a solid white 96 wells

plate and 35 µl of the lysis solution was transferred to the plate. Plates were mixed, briefly centrifuged and left at room temperature for 8 h before counting in a MicroBeta plate counter (Perkin Elmer). Cells have been tested negative for mycoplasma contamination.

Sample size determination and blinding
No statistical methods were applied to predetermine sample size for in vivo pharmacology experiments. Sample sizes were determined on the basis of previous experience with related experimental setups[75]. Studies were not blinded.

Statistical analysis
Statistical analyses were performed using GraphPad Prism v.9.5.1 or SPSS v.29.0.2.0 (IBM). Sample numbers and statistical analysis methods are provided in the figure legends. Data are presented as mean ± s.e.m. unless otherwise specified.

Reporting summary
Further information on research design is available in the Nature Portfolio Reporting Summary linked to this article.

Data availability
snRNA-seq data have been deposited to the NCBI Gene Expression Omnibus under accession number GSE276735. Source data are provided with this paper.

Code availability
The source code used to analyse the snRNA-seq data and produce figures is available at https://github.com/perslab/Sass-2024/.

63. Cheng, W. et al. Calcitonin receptor neurons in the mouse nucleus tractus solitarius control energy balance via the non-aversive suppression of feeding. *Cell Metab.* **31**, 301–312.e5 (2020).
64. Zhang, Q. et al. The glucose-dependent insulinotropic polypeptide (GIP) regulates body weight and food intake via CNS-GIPR signaling. *Cell Metab.* **33**, 833–844.e5 (2021).
65. Fischer, A. W., Schlein, C., Cannon, B., Heeren, J. & Nedergaard, J. Intact innervation is essential for diet-induced recruitment of brown adipose tissue. *Am. J. Physiol.* **316**, E487–E503 (2019).
66. Shi, H. et al. Skeletal muscle O-GlcNAc transferase is important for muscle energy homeostasis and whole-body insulin sensitivity. *Mol. Metab.* **11**, 160–177 (2018).
67. Negoita, F. et al. CaMKK2 is not involved in contraction-stimulated AMPK activation and glucose uptake in skeletal muscle. *Mol. Metab.* **75**, 101761 (2023).
68. Dowsett, G. K. C. et al. A survey of the mouse hindbrain in the fed and fasted states using single-nucleus RNA sequencing. *Mol. Metab.* **53**, 101240 (2021).
69. Fleming, S. J. et al. Unsupervised removal of systematic background noise from droplet-based single-cell experiments using CellBender. *Nat. Methods* **20**, 1323–1335 (2023).
70. Stuart, T. et al. Comprehensive integration of single-cell data. *Cell* **177**, 1888–1902.e21 (2019).
71. Germain, P.-L., Lun, A., Garcia Meixide, C., Macnair, W. & Robinson, M. D. Doublet identification in single-cell sequencing data using scDblFinder. *F1000Research* **10**, 979 (2021).
72. Amezquita, R. A. et al. Orchestrating single-cell analysis with Bioconductor. *Nat. Methods* **17**, 137–145 (2020).
73. Tyssowski, K. M. et al. Different neuronal activity patterns induce different gene expression programs. *Neuron* **98**, 530–546.e11 (2018).
74. Nicol, P. B. et al. Robust Identification of Perturbed Cell Types in Single-Cell RNA-Seq Data. Preprint at *bioRxiv* https://doi.org/10.1101/2023.05.06.539326 (2023).
75. Sveidahl Johansen, O. et al. Lipolysis drives expression of the constitutively active receptor GPR3 to induce adipose thermogenesis. *Cell* **184**, 3502–3518.e33 (2021).
76. Sherry, S. T., Ward, M. & Sirotkin, K. dbSNP-database for single nucleotide polymorphisms and other classes of minor genetic variation. *Genome Res.* **9**, 677–679 (1999).
77. Purcell, S. et al. PLINK: a tool set for whole-genome association and population-based linkage analyses. *Am. J. Hum. Genet.* **81**, 559–575 (2007).
78. Ghoussaini, M. et al. Open targets genetics: systematic identification of trait-associated genes using large-scale genetics and functional genomics. *Nucleic Acids Res.* **49**, D1311–D1320 (2021).
79. Machiela, M. J. & Chanock, S. J. LDlink: a web-based application for exploring population-specific haplotype structure and linking correlated alleles of possible functional variants. *Bioinformatics* **31**, 3555–3557 (2015).
80. Barbeira, A. N. et al. Exploring the phenotypic consequences of tissue specific gene expression variation inferred from GWAS summary statistics. *Nat. Commun.* **9**, 1825 (2018).
81. Barbeira, A. N. et al. Exploiting the GTEx resources to decipher the mechanisms at GWAS loci. *Genome Biol.* **22**, 49 (2021).

Article

82. Gamazon, E. R. et al. A gene-based association method for mapping traits using reference transcriptome data. *Nat. Genet.* **47**, 1091–1098 (2015).
83. Jurgens, S. J. et al. Adjusting for common variant polygenic scores improves yield in rare variant association analyses. *Nat. Genet.* **55**, 544–548 (2023).
84. Chen, J. et al. The trans-ancestral genomic architecture of glycemic traits. *Nat. Genet.* **53**, 840–860 (2021).
85. Pagès, H. SNPlocs.Hsapiens.dbSNP144.GRCh37: SNP locations for *Homo sapiens* (dbSNP Build 144). R package version 0.99.20 https://doi.org/10.18129/B9.bioc.SNPlocs.Hsapiens. dbSNP144.GRCh37 (2017).
86. Hormozdiari, F., Kostem, E., Kang, E. Y., Pasaniuc, B. & Eskin, E. Identifying causal variants at loci with multiple signals of association. *Genetics* **198**, 497–508 (2014).
87. Bjerregaard, P. et al. Inuit health in Greenland: a population survey of life style and disease in Greenland and among Inuit living in Denmark. *Int. J. Circumpolar Health* **62**, 3–79 (2003).
88. Andersen, M. K. et al. The derived allele of a novel intergenic variant at chromosome 11 associates with lower body mass index and a favorable metabolic phenotype in Greenlanders. *PLoS Genet.* **16**, e1008544 (2020).
89. Zhou, X. & Stephens, M. Genome-wide efficient mixed-model analysis for association studies. *Nat. Genet.* **44**, 821–824 (2012).

Author contributions Conceptualization was done by F.S., T.M., J.B.H., T.W.S. and Z.G.-H. The peptide chemistry design campaign was led by J.B.H., M.T.-C. and M.B.F.G. The macaque study was conducted by L.B., M.K. and P.K. In vivo methodology was developed by K.A.S. and T.S.N. Human genetics analysis was carried out by M.K.A., M.S., Y.W., M.G.U., M.E.J., I.M., A.A., N.G., T.H., M.M.B. and T.O.K. In vivo mouse phenotyping studies were carried out by F.S., T.M., J.H.E., H.B.B., T.S.N., J.M.B., L.D., W.T.Y., C.K.K., A.J.T., S. Kernodle, K.A.S., C.T.V., W.I.h.P., A.L.B., M.G.-M., D.M.R., T.H.P., P.C.N.R., R.J.S., A.W., J.H., S. Kooijman and J.B.H. In situ hybridization was conducted by O.D. Pharmacological cell signalling studies were carried out by D.P.C., J.E.P., T.W.S. and A.P. Graphical visualization was done by F.S. The original draft was written by F.S., T.M., J.B.H., T.W.S. and Z.G.-H. The manuscript was edited and revised by all co-authors.

Competing interests T.M., J.H.E., J.B.H., D.P.C., M.B.F.G., M.T.-C., T.W.S. and Z.G.-H. work or have worked in some capacity for Embark Laboratories ApS, a company developing therapeutics for the treatment of T2D and obesity. P.K. is a consultant for Embark Laboratories ApS. The use of and chemical composition for NK2R agonists are patented by the University of Copenhagen and Embark Laboratories ApS, respectively. R.J.S. has received research support from Novo Nordisk, Fractyl, AstraZeneca, Congruence Therapeutics, Eli Lilly, Bullfrog AI, Glycsend Therapeutics and Amgen. R.J.S. has served as a paid consultant for Novo Nordisk, Eli Lilly, CinRx, Fractyl, Structure Therapeutics, Crinetics and Congruence Therapeutics. R.J.S. has equity in Calibrate, Rewind and Levator Therapeutics. The other authors declare no competing interests.

Additional information
Supplementary information The online version contains supplementary material available at https://doi.org/10.1038/s41586-024-08207-0.
Correspondence and requests for materials should be addressed to Jakob B. Hansen or Zachary Gerhart-Hines.
Peer review information *Nature* thanks the anonymous reviewer(s) for their contribution to the peer review of this work.
Reprints and permissions information is available at http://www.nature.com/reprints.

a Gq-signalling and HbA1c associations of *NK2R* missense variants
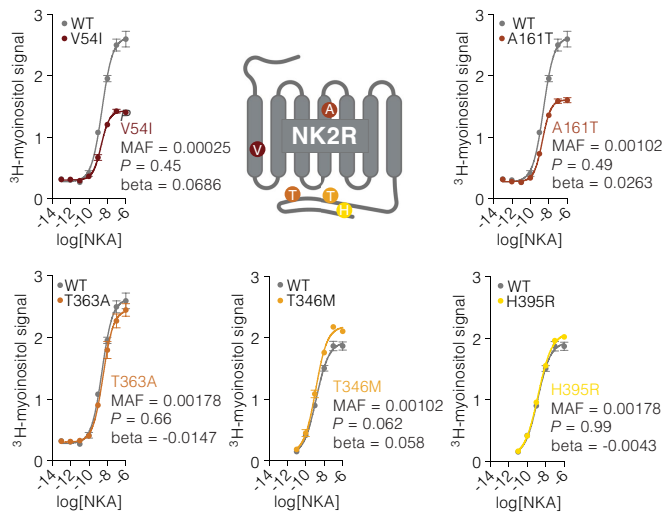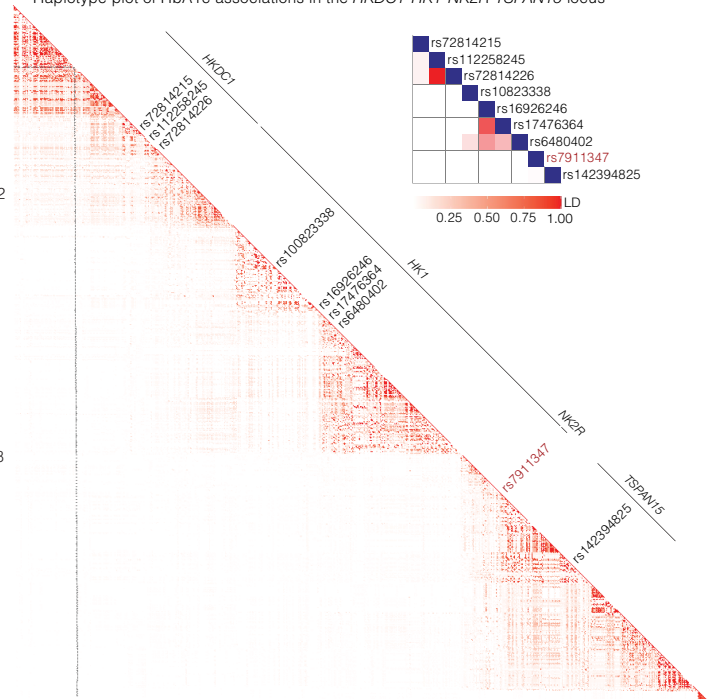
b Haplotype plot of HbA1c associations in the *HKDC1-HK1-NK2R-TSPAN15* locus

Extended Data Fig. 1 | Effect of *NK2R* genetic variants on receptor signaling. a, Gq signalling and HbA1c associations of *NK2R* missense variants, V54I, A161T, T363A, T346M and H395R, (n = 2 per variant). **b**, Haplotype plot of HbA1c associations in the *HKDC1-HK1-NK2R-TSPAN15* locus. Data are represented as mean ± s.e.m. Two-sided association tests without multiple corrections, **a**.
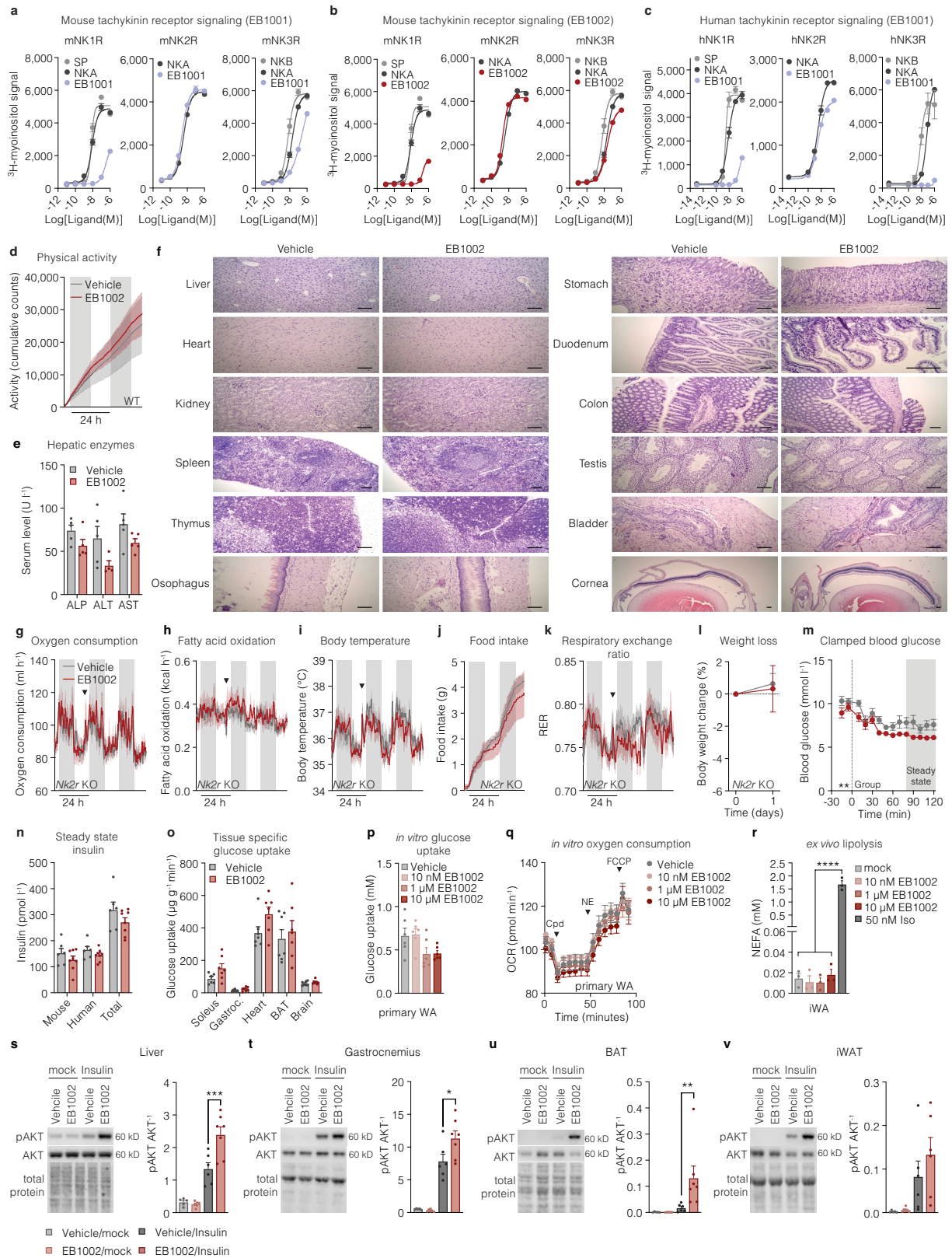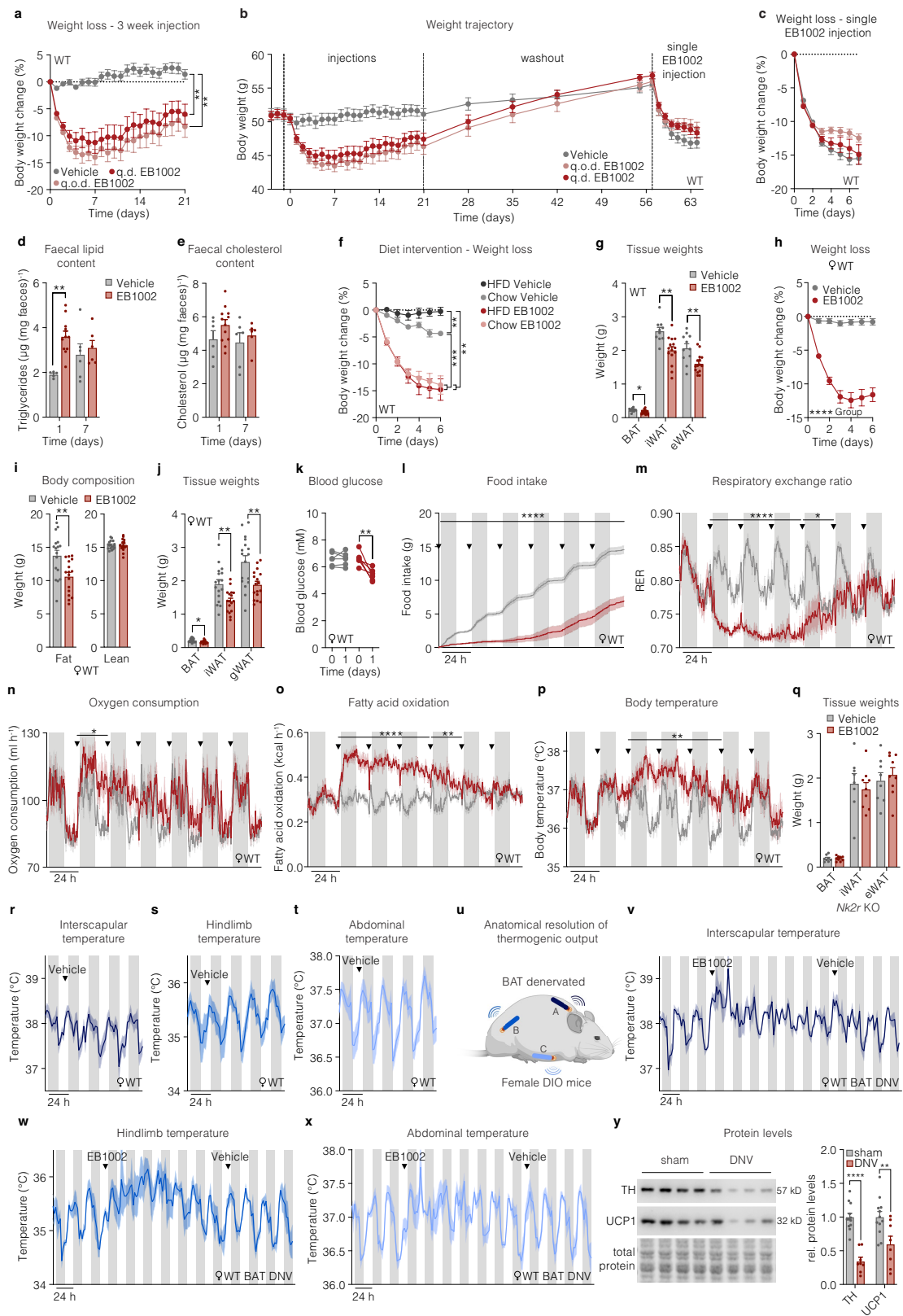
Extended Data Fig. 2 | See next page for caption.

Extended Data Fig. 2 | Development and acute testing of NK2R selective agonists. a, Mouse tachykinin receptor signaling with endogenous ligands and EB1001, **b**, mouse tachykinin receptor signaling with endogenous ligands and EB1002, and, **c**, human tachykinin receptor signaling with endogenous ligands and EB1001, (n = 2 per variant for a-c). **d**, Cumulative locomotor activity of DIO mice following a single injection of vehicle (n = 6 mice) or 325 nmol/kg (n = 5 mice). **e**, Serum liver enzymes (n = 4 (ALT EB1002), n = 5 mice for remaining data) and **f**, representative microscopy images of various tissues of CD-1 mice after injections with vehicle or increasing concentrations of EB1002 (see methods, 7500 nmol/kg EB1002 prior to euthanasia), scale bars 100 μm. **g**, Oxygen consumption, **h**, fatty acid oxidation, **i**, body temperature, **j**, food intake, **k**, RER, and, **l**, weight loss of DIO *Nk2r* KO mice following a single injection of vehicle or 325 nmol/kg EB1002 (n = 6 mice per group for e, f, h-j, l, n = 5 mice per group for g), downward triangles signify time of injection. **m**, clamped blood glucose, **n**, steady state mouse and human insulin levels and **o**, glucose uptake into metabolically active tissues for a hyperinsulinemic-euglycemic clamp of lean mice following a single injection of vehicle (n = 7 mice) or 325 nmol/kg EB1002 (n = 8 mice). **p**, in vitro glucose uptake (n = 6 each condition) and **q**, oxygen consumption of primary white adipocytes (WA) in response to various concentrations of EB1002 (n = 6 (vehicle), n = 8 (each EB1002 concentration)). **r**, ex vivo lipolysis of mature inguinal WA in response to various concentrations of EB1002 and 50 nM isoproterenol (n = 3 each condition). Representative western blot images and quantification of **s**, liver, **t**, gastrocnemius, **u**, BAT and, **v**, iWAT of DIO mice treated with vehicle or 325 nmol/kg EB1002 18 h prior to injections with a mock solution or insulin (n = 5 (vehicle/mock), n = 6 (EB1002/mock, vehicle/insulin) n = 7 mice (EB1002/insulin)). Data are represented as mean ± s.e.m. For all: *P < 0.05, **P < 0.01, ***P < 0.005, ****P < 0.0001. Unpaired two-tailed *t*-test of AUC for 48 h after injection, **d, g-k**; unpaired two-tailed *t*-test, **e, l, n, o**; repeated measures two-way ANOVA with Geisser-Greenhouse correction, significance indicates treatment effect, **m**; ordinary one-way ANOVA with Tukey's multiple comparisons test, significance shows post hoc test for treatment effect, **p, r**; ordinary one-way ANOVA of AUC for baseline, compound (cpd), NE and FCCP increments, **q**; and ordinary two-way ANOVA with Sidak's multiple comparison, significance indicates post hoc test between vehicle and EB1002 treated mice, **s-v**. Uncropped blots are presented in Supplementary Fig. 1.

Extended Data Fig. 3 | See next page for caption.

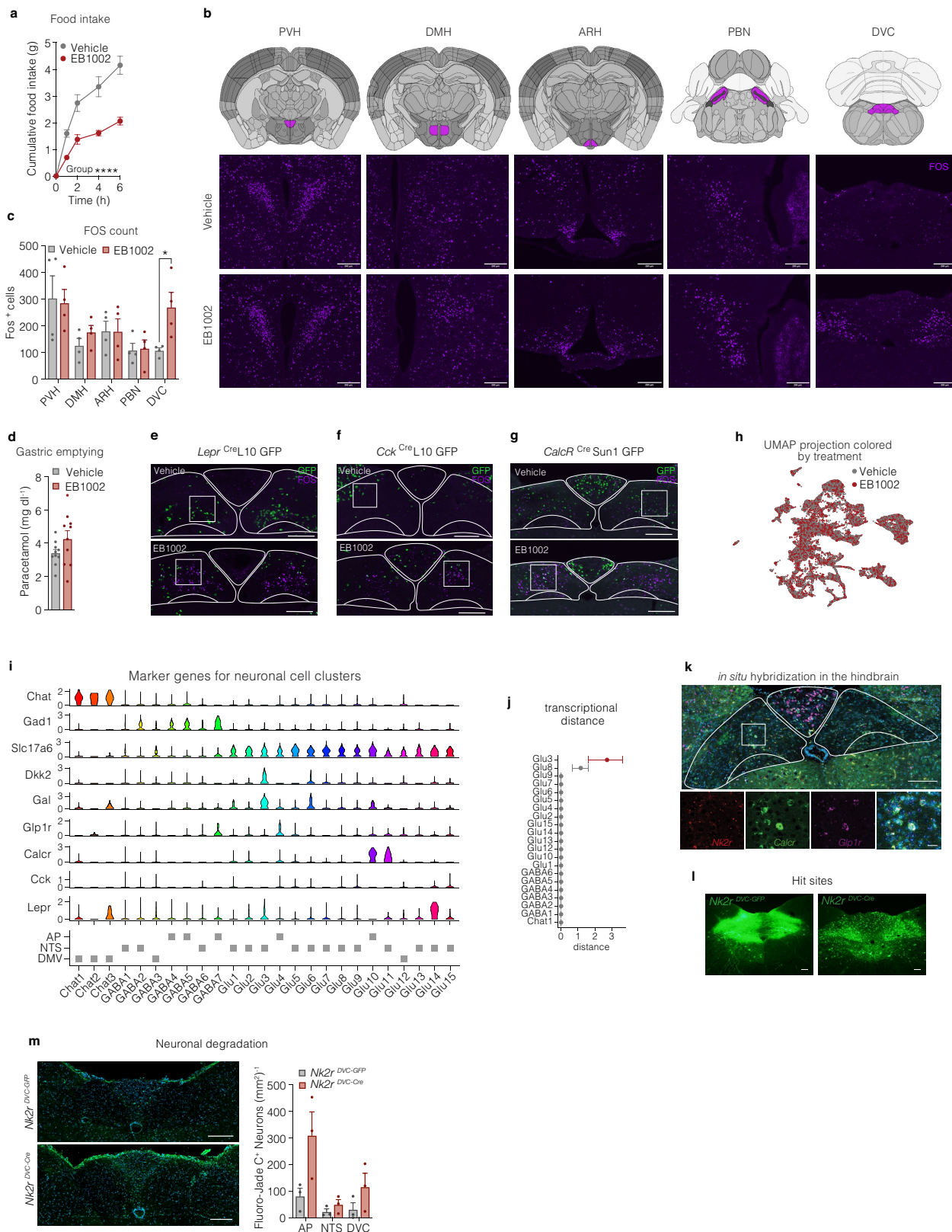**Extended Data Fig. 3 | In vivo effects of repeated NK2R agonist dosing.**
a, Weight loss of DIO mice that have been injected s.c. daily with vehicle or 325 nmol/kg EB1002 (q.d. EB1002), or every other day with 325 nmol/kg EB1002 (q.o.d. EB1002) (n = 10 mice per group), and **b**, weight trajectory of the same mice including a washout period and a single re-injection with 325 nmol/kg EB1002, with **c**, weight loss after re-injection. **d**, Faecal lipid content and **e**, faecal cholesterol content of DIO mice that have been injected s.c. daily with vehicle or 325 nmol/kg EB1002 (n = 6 mice (d1 vehicle and d7 vehicle and EB1002), n = 12 mice (d1 EB1002)). **f**, Weight loss of DIO mice that were transitioned to chow diet or continued on HFD 5 days prior to daily s.c. injections with vehicle or 325 nmol/kg EB1002, data normalized to d0 (n = 6 mice (HFD vehicle), n = 8 mice (chow vehicle, chow EB1002 and HFD EB1002)). **g**, Adipose tissue weights of DIO mice that have been injected s.c. daily with vehicle (n = 11 mice) or 325 nmol/kg EB1002 (n = 15 mice) for 7 days. **h**, Weight loss, **i**, body composition, **j**, adipose depot weights, **k**, blood glucose, **l**, food intake, **m**, RER, **n**, oxygen consumption, **o**, fatty acid oxidation, and **p**, body temperature of female DIO mice that have been injected s.c. daily with vehicle or 325 nmol/kg EB1002 (n = 6 mice per group (f, I, j-m), n = 17 mice per group (g, h), n = 6 mice (vehicle) and n = 5 mice (EB1002) for n), downward triangles signify time of injection. **q**, Adipose depot weights of DIO *Nk2r* KO mice that have been injected s.c. daily with vehicle (n = 8 mice) or 325 nmol/kg EB1002

(n = 9 mice). **r**, Interscapular temperature (n = 3 mice), **s**, hindlimb temperature (n = 5 mice), **t**, abdominal temperature (n = 5 mice) of DIO mice after a single s.c. injection of vehicle, downward triangles signify time of vehicle injection. **u**, Schematic setup of triple chip study to interrogate anatomical resolution of thermogenic output with **v**, interscapular temperature, **w**, hindlimb temperature, and **x**, abdominal temperature of BAT denervated DIO mice after a single injection of 325 nmol/kg EB1002 and vehicle (n = 3 mice), downward triangles signify time of injection of the indicated compound. **y**, Representative western blot images and quantification of BAT from sham operated or BAT denervated mice (n = 6 (sham), n = 4 mice (DNV), each BAT lobe has been analyzed separately). Data are represented as mean ± s.e.m. For all: *P < 0.05, **P < 0.01, ***P < 0.005, ****P < 0.0001. Repeated measures two-way ANOVA with Geisser-Greenhouse correction and Tukey's multiple comparison test, significance indicates post hoc test for treatment effect at last timepoint, **a, f**; repeated measures two-way ANOVA with Geisser-Greenhouse correction, significance indicates treatment effect, **c, h**; repeated measures two-way ANOVA with Geisser-Greenhouse correction and Sidak's multiple comparison test, significance indicates post hoc test for treatment effects, **d, e**; unpaired two-tailed *t*-test, **g, i, j, q, y**; repeated measures two-way ANOVA and Sidak's multiple comparison, significance indicates time effect, **k**; unpaired two-tailed *t*-test of AUC of 24 h increments, **l-p**.
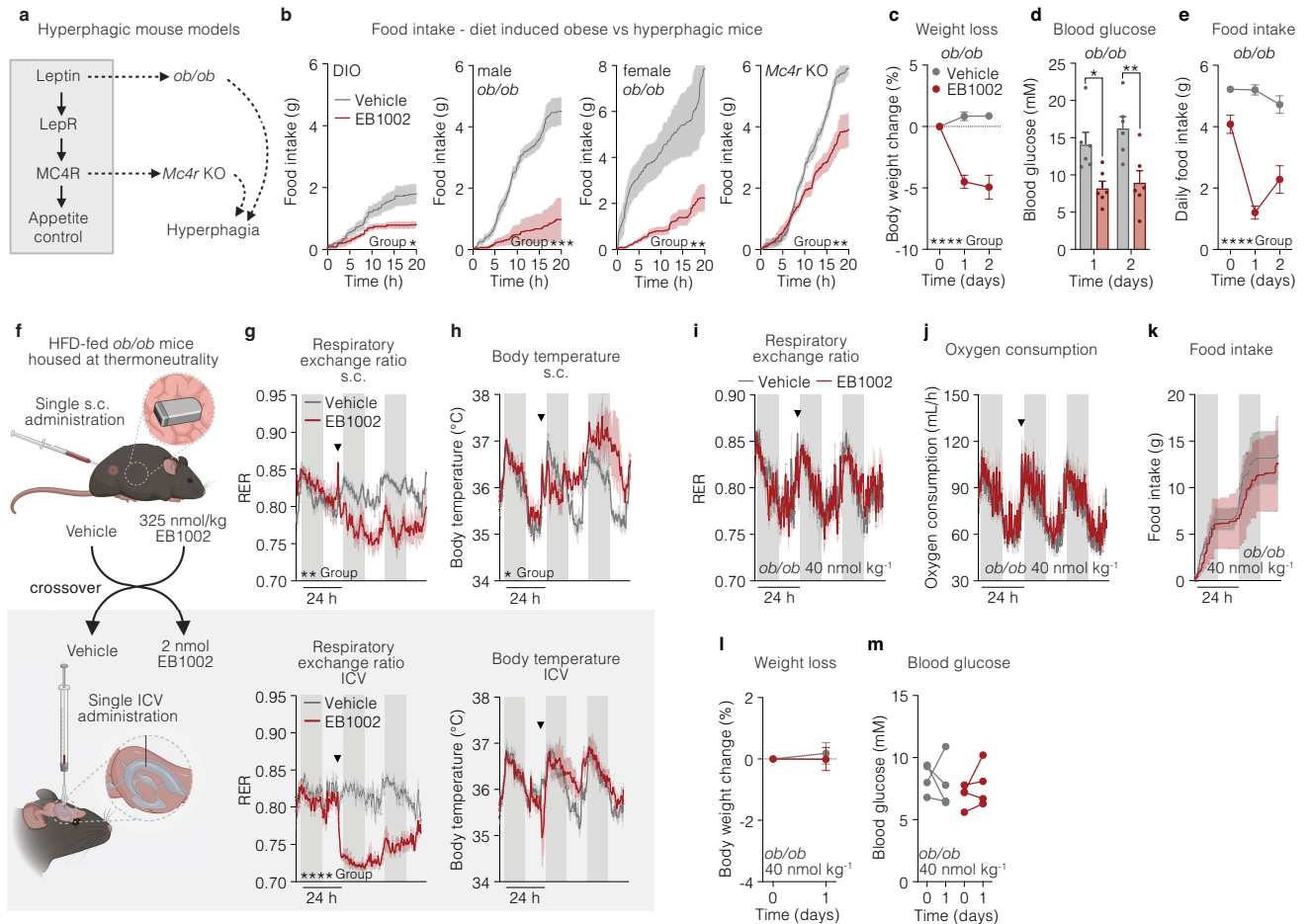
Extended Data Fig. 4 | Anatomical resolution of NK2R agonism. a, Genetic models of hyperphagic obesity used to interrogate NK2R agonist-dependent appetite suppression. **b**, Food intake following a single s.c. administration of vehicle or 325 nmol/kg EB1002 to DIO, male and female leptin deficient (*ob/ob*) and *Mc4r* KO mice (n = 6 mice (DIO, vehicle), n = 5 mice (DIO, EB1002), n = 8 mice (male *ob/ob*, vehicle; female *ob/ob*), n = 6 mice (male *ob/ob*, EB1002), n = 11 mice (*Mc4r* KO, vehicle), n = 8 mice (*Mc4r* KO, EB1002)). **c**, Weight loss, **d**, blood glucose and **e**, food intake of ob/ob mice housed at thermoneutrality following a single s.c. injection of vehicle or 325 nmol/kg EB1002 (n = 6 mice each group). **f**, Schematic of crossover study comparing in vivo effects of peripheral versus central delivery of EB1002 on **g**, RER, **h**, body temperature following s.c. or ICV injection (n = 6 (vehicle s.c injections and EB1002 ICV injections), n = 4 (EB1002

s.c. injections and vehicle ICV injections)), downward triangles signify time of injection (g, h). **i**, RER, **j**, oxygen consumption, **k**, food intake, **l**, weight loss and **m**, blood glucose of *ob/ob* mice following a single s.c. injection of vehicle or 40 nmol/kg EB1002 (n = 4 mice each group). Data are represented as mean ± s.e.m. For all: *P ≤ 0.05, **P < 0.01, ***P < 0.005, ****P < 0.0001. Unpaired two-tailed *t*-test of AUC **b**; Repeated measures two-way ANOVA with Geisser-Greenhouse correction, significance indicates treatment effect, **c, e**; Repeated measures two-way ANOVA with Sidak's multiple comparison test, significance shows post hoc test for treatment effects, **d**; unpaired two-tailed *t*-test of AUC for 48 h after injection, **g-k**; unpaired two-tailed *t*-test, **l**; Repeated measures two-way ANOVA, **m**.

a Food intake

b PVH   DMH   ARH   PBN   DVC

c FOS count

d Gastric emptying

e *Lepr*^Cre^L10 GFP

f *Cck*^Cre^L10 GFP

g *CalcR*^Cre^Sun1 GFP

h UMAP projection colored by treatment

i Marker genes for neuronal cell clusters

j transcriptional distance

k *in situ* hybridization in the hindbrain

l Hit sites

m Neuronal degradation

Extended Data Fig. 5 | See next page for caption.

Article

Extended Data Fig. 5 | Central effects of NK2R agonism. a, Food intake in over-night fasted mice that have been s.c. injected with vehicle or 325 nmol/kg EB1002 at time of refeeding (n = 10 mice per group). **b**, Schematics of brain sections (adopted from The Allen Brain Atlas) and representative images of FOS staining (purple) with **c**, quantification of FOS positive cells in the paraventricular nucleus of the hypothalamus (PVH), the dorsomedial hypothalamic nucleus (DMH), arcuate nucleus (ARH), the parabrachial nucleus (PBN) and the dorsal vagal complex (DVC) of overnight fasted mice injected with vehicle or 325 nmol/kg EB1002 2 h prior to euthanasia (n = 4 mice per group), scale bar 200 μm. **d**, Liquid phase gastric emptying of mice s.c. injected with vehicle or 325 nmol/kg EB1002 (n = 10 mice each group). Representative microscopy images and quantification of FOS (purple) colocalization with reporter neurons (green) in the DVC of **e**, *Lepr*^Cre L10 GFP (n = 3 (vehicle), n = 6 (EB1002)), **f**, *Cck*^Cre L10 GFP (n = 2 (vehicle), n = 3 (EB1002)), and, **g**, *Calcr*^Cre Sun1 GFP mice (n = 6 (vehicle), n = 7 (EB1002)) injected with vehicle or EB1002, scale bar 200 μm. **h**, UMAP plot of 23,664 neurons colored by treatment, **i**, violin plot, and **j**, transcriptional case-control analysis of single nuclei RNA sequencing data of the DVC of mice s.c. injected with vehicle or 325 nmol/kg EB1002 2 h prior to euthanasia (n = 6 samples with 5 mice/sample). **k**, in situ hybridization of *Nk2r* (red), *Calcr* (green) and *Glp1r* (purple) in the DVC, scale bar: top panel 200 μm, bottom panel 50 μm. **l**, Representative microscopy images of the hit sites, scale bar 200 μm. **m**, Representative microscopy images of Fluoro-Jade C stain in the DVC of *Nk2r* floxed mice that received a bilateral injection of AAV-GFP (*Nk2r*^DVC-GFP) or AAV-Cre (*Nk2r*^DVC-Cre) into the DVC, scale bar 200 μm, (n = 3 mice per group). Data are represented as mean ± s.e.m. For all: *P ≤ 0.05, **P < 0.01, ***P < 0.005, ****P < 0.0001. Repeated measures two-way ANOVA with Geisser-Greenhouse correction, significance indicates treatment effect, **a**; unpaired two-tailed *t*-test, **c, d, m**; for **j** red color indicates *P < 0.05.
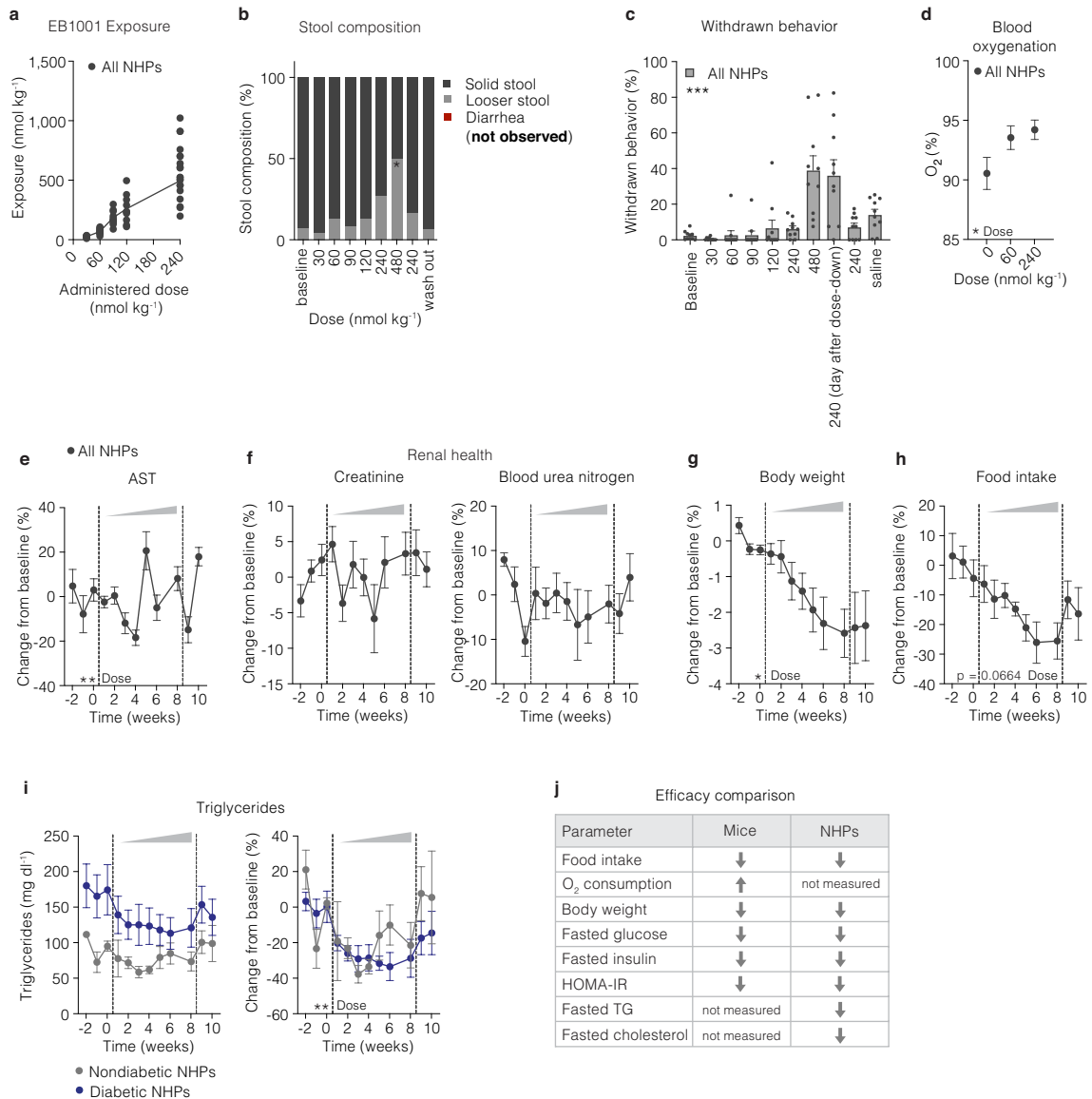
Extended Data Fig. 6 | Effects of NK2R agonism in nonhuman primates.
a, Exposure to EB1001 after s.c. injections of different doses. **b**, stool
composition, **c**, changes in withdrawn behaviour, **d**, blood oxygenation,
e, blood aspartate transaminase (AST), **f**, creatinine and blood urea nitrogen
levels, **g**, body weight, and **h**, food intake during the dose escalation study
(n = 10 nonhuman primates (NHPs) for a-h). **i**, Changes in triglycerides (raw-left
side and %-right side), normoglycemic (n = 3 NHPs) and diabetic NHPs (n = 7

NHPs). **j**, Summary comparison of effects of NK2R agonism between mice and
NHPs. Data are represented as mean ± s.e.m. For all: *P < 0.05, **P < 0.01,
***P < 0.005, ****P < 0.0001. Repeated measures one-way ANOVA with
Geisser-Greenhouse correction and Dunnett's multiple comparison test,
significance indicates post-test between vehicle and treatments, **b**; repeated
measures one-way ANOVA with Geisser-Greenhouse correction, **c-h**; Repeated
measures two-way ANOVA with Geisser-Greenhouse correction, **i**.

Article

Extended Data Table 1 | Associations of *NK2R* variants R3232H (rs61732393-T), I23T (rs5030920-G), V54I (rs151093941-T) and A161T (rs148031991-T) with cardiometabolic traits and minor allele frequencies (MAF) in five different ancestries

Trait	P-value	Beta	Standard error	Sample size	PMID
R3232H (rs61732393-T)					
HbA1c	0.0003	0.1300	0.0358	437,749	34226706
Non-HDLc	0.0412	0.0592	0.0290	810,161	34887591
HOMA-IR	0.0342	-0.2033	0.0960	9,349	31118516
Random glucose	0.0472	0.0568	0.0286	400,775	36959364
Systolic blood pressure	0.0310	1.1861	0.5499	459,133	36959364
Diastolic blood pressure	0.0253	0.2853	0.1275	19,429	28270201
I23T (rs5030920-G)					
HbA1c	1.50e-23	0.0223	0.0022	437,749	34226706
Total bilirubin	3.30e-10	-0.0114	0.0018	436,055	34226706
AST-ALT ratio	7.49e-7	-0.0139	0.0028	354,455	33462484
Direct bilirubin	0.0007	-0.0077	0.0023	372,739	34226706
BMI-adjusted WHR	0.0013	0.0091	0.0028	348,902	30239722
Triglycerides	4.13e-05	-0.0061	0.0015	1,495,680	34887591
Peripheral artery disease	0.0027	-0.0582	0.0194	Case: 12,086 Control: 449,548	34601942
ALT	0.0015	0.0080	0.0025	437,724	34226706
Fasting glucose	0.0037	-0.0140	0.0048	36,475	33402679
Kidney volume	0.0043	0.0214	0.0075	32,860	34128465
Triglycerides levels in non-T2D	0.0046	-0.0073	0.0026	402,944	36269708
Hypothyroidism	0.0046	0.001	0.0006	408,963	30297966
Right ventricular stroke volume to left ventricular stroke volume ratio	0.0082	0.0225	0.0085	41,135	35697867
Waist-hip ratio in females	0.04055	0.0057	0.0028	350,672	25673412
Non-HDL cholesterol	0.0163	0.0047	0.0020	925,745	34887591
BMI-adjusted T2D	0.0446	-0.0165	0.0082	129,380	29632382
Neuropathy in T2D	0.0207	-0.1725	0.0745	2,344	36653562
Primary sclerosing cholangitis	0.0231	-0.0926	0.0407	9,269	27992413
Peripheral artery disease	0.0240	-0.0583	0.0258	23,418	34601942
Right ventricular stroke volume	0.0270	0.0155	0.0070	41,135	35697867
Heart failure	0.0082	0.0249	0.0094	175,728	31919418
Short sleep duration	0.0280	-0.0025	0.0011	315,267	30846698
Corneal resistance factor	0.0290	-0.0256	0.0117	76,029	33311554
Photoreceptor cell layer thickness	0.0307	0.0205	0.0095	31,135	36848389
Arm-fat ratio	0.0334	0.0012	0.0006	116,138	30664634
Right ventricular end-diastolic volume to left	0.0320	0.0173	0.0081	41,135	35697867
Right ventricular end-diastolic volume to left ventricular end-diastolic volume ratio	0.0320	0.0173	0.0081	41,135	35697867
Daytime napping	0.0360	-0.0021	0.0015	452,633	33568662
Systolic blood pressure	0.0233	0.0045	0.0020	731,483	30224653
Neuromyelitis optica (AQP4-IgG negative)	0.03786	-0.4600	0.2203	233	29769526
BMI-adjusted HbA1c	0.01393	0.0116	0.0047	131,082	34059833
Kidney stone disease	0.03944	-0.0280	0.0136	70,082	37980427
Insomnia (ICD defined)	0.0419764	0.0574	0.0282	14,773	33893285
Short-axis pulmonary artery (cm), BSA indexed	0.042	-0.0172	0.0085	41,135	35697867
Pulmonary artery to aorta ratio, systole	0.042	-0.0182	0.0089	41,135	35697867
Dernatophytosis	0.04468	-0-0431	0.0215	26,542	33893285
BMI-adjusted insulin sensitivity index	0.04812	-0.0250	0.0126	16,735	33893285
Calcific aortic stenosis	0.04849	-0.0333	0.0168	53,900	37038246
Large artery stroke	0.03035	0.0549	0.0253	25,464	36180795
BMI-adjusted fasting insulin in males	0.0065128	0.0595	0.0219	7,286	28119442
T2D	0.02137	-0.0558	0.0243	22,074	33188205
V54I (rs151093941-T)					
HbA1c (mmol/L)	0.0190	-2.7857	1.1867	1,997	28588112
Triglyceride levels in individuals without type 2 diabetes	0.0209	-0.3647	0.1579	402,944	36269708
Height	0.0390	-0.1286	0.0623	458,235	34226706
A161T (rs148031991-T)					
Fasting insulin	0.0067	0.7683	0.2834	7,193	29040543
Hypothyroidism	0.0420	0.0175	0.0086	408,963	30297966
BMI-adjusted Leptin	0.0434	0.1637	0.0811	49,830	32917775

African American (AFR), Admixed American (AMR), East Asian (EAS), European (EUR) and South Asian (SAS). The beta (effect size), standard error, p-value and sample size are from the largest published European study for each trait, referenced with their PubMed ID (PMID). The association tests were two-sided without multiple corrections. HbA1c: Glycated hemoglobin; Non-HDLc: Non High-Density Lipoprotein Cholesterol; HOMA-IR: homeostatic model assessment – insulin resistance; AST-ALT ratio: Aspartate transferase - alanine transaminase ratio; BMI: body mass index; WHR: Waist-hip ratio; ALT: Alanine transaminase.

Extended Data Table 2 | Burden tests results for HK1, NK2R and TSPAN15 from Genebass

Gene	HK1			NK2R			TSPAN15		
Burden test	Burden Beta (P-value)	SKAT Beta (P-value)	SKAT-O Beta (P-value)	Burden Beta (P-value)	SKAT Beta (P-value)	SKAT-O Beta (P-value)	Burden Beta (P-value)	SKAT Beta (P-value)	SKAT-O Beta (P-value)
pLoF	-3.82e-02 (2-01e-12)	-3.82e-02 (9.42e-06)	-3.82e-02 (1.93e-12)	6.11e-04 (8.14e-01)	6.11e-04 (9.27e-01)	6.11e-04 (1.00)	-9.65e-04 (8.22e-01)	-9.65e-04 (4.86e-01)	-9.65e-04 (6.88e-01)
Missense	-2.28e-3 (1.65e-03)	-2.28e-3 (1.17e-03)	-2.28e-3 (4.14e-04)	2.55e-04 (3.77e-01)	2.55e-04 (9.37e-02)	2.55e-04 (1.45e-01)	8.59e-05 (8.65e-01)	8.59e-05 (2.08e-01)	8.59e-05 (3.38e-01)
Synonymous	2.82e-4 (4.47e-01)	2.82e-4 (8.20e-01)	2.82e-4 (6.60e-01)	1.74e-03 (3.58e-01)	1.74e-03 (2.44e-02)	1.74e-03 (4.36e-03)	-4.44e-04 (7.28e-01)	-4.44e-04 (7.47e-01)	-4.44e-04 (8.98e-01)

				NK2R rare coding variants				
Variant	Base pair location	A1	A0	Consequence	A1 frequency	Beta		P-value
10:71168778	10:71168778	A	C	Missense (Ala184Ser)	1.3588E-06	2.9585		0.0012
10:71166871	10:71166871	A	G	Missense (Ser343Phe)	2.7177E-06	2.0099		0.0018
10:71168711	10:71168711	C	G	Missense (Thr394Ser)	4.1047E-06	1.9410		0.0026
rs61732393	10:71168687	T	C	Missense (Arg323His)	0.0009	0.1053		0.0033
10:71175965	10:71175965	A	G	Missense (Thr21Met)	1.4949E-05	-0.7807		0.0045
rs372747490	10:71175734	A	G	Missense (Thr20Ile)	2.7179E-06	-1.6760		0.0093
10:71174874	10:71174874	C	A	Synonymous (Leu143=)	1.3588E-06	-2.2969		0.0117
rs1332935976	10:71164658	T	C	Synonymous (Val253=)	2.7177E-06	-1.6149		0.0122
rs144577707	10:71176027	G	A	Missense (Phe214Ser)	0.0010	-0.0819		0.0126
rs1339554180	10:71164750	A	T	Missense (Asn303Tyr)	1.3588E-06	-2.2511		0.0135
rs779892027	10:71164684	T	A	Synonymous (Gly236=)	2.1742E-05	0.5093		0.0149
10:71168708	10:71168708	A	G	Synonymous (Ala244=)	1.3668E-06	2.2179		0.0150
rs1229281458	10:71166951	A	C	Missense (Ala39Ser)	1.3588E-06	-2.2056		0.0155
rs1043747700	10:71166904	T	C	Missense (Ala116Thr)	5.4354E-06	1.0387		0.0227
rs1277064736	10:71175719	A	G	Synonymous (Pro138=)	1.4947E-05	-0.6198		0.0241
10:71164823	10:71164823	T	C	Missense (Gly374Glu)	1.3588E-06	2.0333		0.0257
rs201729201	10:71174774	T	C	Missense (Ser18Asn)	5.4359E-06	1.0131		0.0262
rs117605989	10:71175704	A	G	Synonymous (Ser343=)	0.0047	0.0343		0.0264
rs1419007427	10:71166993	A	G	Synonymous (Pro365=)	5.4356E-06	1.0011		0.0281
rs746711930	10:71164779	G	GGCACCGTGC	Inframe deletion (His235_Ala237del)	4.0765E-06	1.1523		0.0286
rs1276711225	10:71175937	C	T	Missense (Gln276Arg)	2.7177E-06	-1.4060		0.0292
10:71167027	10:71167027	C	G	Missense (Leu292Val)	1.3588E-06	-1.9595		0.0316
rs1010580037	10:71174872	C	T	Missense (Ile121Val)	1.0871E-05	0.6429		0.0344
10:71174787	10:71174787	T	C	Missense (Arg319Gln)	2.7177E-06	-1.3294		0.0392
rs146283790	10:71168778	T	C	Missense (Val172Ile)	1.0871E-05	0.5617		0.0410
rs199995772	10:71166871	T	C	Missense (Ala126Thr)	2.7177E-06	1.0581		0.0444
10:71168711	10:71168711	G	C	Missense (Cys262Ser)	4.0765E-06	1.0479		0.0465
10:71168687	10:71168687	T	C	Missense (Asp334Asn)	2.7177E-06	-1.2817		0.0468
10:71175965	10:71175965	T	A	Missense (Val48Glu)	1.3588E-06	1.7957		0.0488
rs142415572	10:71175734	C	T	Missense (Thr251Ala)	3.8047E-05	0.3170		0.0492
10:71174874	10:71174874	C	A	Missense (Phe139Cys)	1.3588E-06	-1.2658		0.0495
10:71164658	10:71164658	A	G	Synonymous (Cys167=)	2.7177E-06	1.2645		0.0498

Three types of burden tests (Burden, SKAT and SKAT-O) for three types of exome variants (pLOF, missense and synonymous) were retrieved. Summary statistics of 9 NK2R synonymous variants are reported. The burden tests were two-sided without multiple corrections. A1: effect allele; A0: other allele; A1 frequency: allele frequency of the effect allele; P: p-value.

Article

Extended Data Table 3 | Summary of association analyses with metabolic traits for rs139900276

	N	Effect size (SE)	P-value
Body composition			
BMI	5750	-0.085 (0.02)	8.6×10^{-5}
Weight	5758	-0.071 (0.02)	0.0012
Waist	5717	-0.082 (0.02)	1.7×10^{-4}
Hip	5716	-0.072 (0.02)	0.0014
Waist-hip-ratio	5714	-0.065 (0.02)	0.0014
Waist-height-ratio	5705	-0.065 (0.02)	5.6×10^{-5}
Fat%	3843	-0.087 (0.03)	7.8×10^{-4}
Glucose homeostasis			
Fasting plasma glucose	4201	-0.024 (0.02)	0.325
2h plasma glucose	3972	0.008 (0.02)	0.747
Fasting serum insulin	4200	-0.058 (0.02)	0.019
2h serum insulin	3973	0.0009 (0.02)	0.971
HbA1c	5117	-0.009 (0.02)	0.656

Effect sizes reported in standard deviations for the rs139900276 CG-allele from association analyses run with an additive model. The association tests were two-sided without multiple corrections.

Extended Data Table 4 | Overview of gross changes in tissue architecture and cellar appearances following pharmacological pre-toxicology study

	Group	Liver	Heart	Kidney	Spleen	Thymus	Esophagus	Stomach	Duodenum	Colon	Testes	Bladder	Eye
ID	Vehicle	01--1	01--2	01--2	01--1	01--5	01--3	01--3	01--3	01--3	01--4	01--5	01--5
ID	EB1002	02--1	02--2	02--2	02--1	02--5	02--3	02--3	02--3	02--3	02--4	02--5	02--5
comp. to vehicle		ncd 1)	ncd	ncd	ncd	ncd	ncd	ncd	ncd	ncd	ncd	ncd 2)	ncd
ID	Vehicle	04--1	04--2	04--2	04--1	04--5	04--3	04--3	04--3	04--3	04--4	04--5	04--5
ID	EB1002	05--1	05--2	05--2	05--1	05--5	05--3	05--3	05--3	05--3	05--4	05--5	05--5
comp. to vehicle		ncd 3)	ncd	ncd	ncd	ncd	ncd	ncd	ncd	ncd	ncd	ncd	ncd 4)
ID	Vehicle	07--1	07--2	07--2	07--1	07--5	07--3	07--3	07--3	07--3	07--4	07--5	07--5
ID	EB1002	08--1	08--2	08--2	08--1	08--5	08--3	08--3	08--3	08--3	08--4	08--5	08--5
comp. to vehicle		ncd	ncd	ncd 5)	ncd	ncd	ncd	ncd	ncd	ncd	ncd	ncd	ncd
ID	Vehicle	10--1	10--2	10--2	10--1	10--5	10--3	10--3	10--3	10--3	10--4	10--5	10--5
ID	EB1002	11--1	11--2	11--2	11--1	11--5	11--3	11--3	11--3	11--3	11--4	11--5	11--5
comp. to vehicle		ncd 6)	ncd	ncd	ncd	ncd	ncd	ncd	ncd	ncd	ncd	ncd	ncd
ID	Vehicle	13--1	13--2	13--2	13--1	13--5	13--3	13--3	13--3	13--3	13--4	13--5	13--5
ID	EB1002	14--1	14--2	14--2	14--1	14--5	14--3	14--3	14--3	14--3	14--4	14--5	14--5
comp. to vehicle		ncd	ncd	ncd 7)	ncd	ncd	ncd	ncd	ncd	ncd	ncd	ncd	ncd

Mice were either injected with vehicle or EB1002 in a dose-up fashion up to 7500 nmol/kg. Tissues were taken for pathohistological evaluation and compared in a pair-wise fashion. Comp. to vehicle – compared to vehicle; ncd – no change detected. 1) slightly increased amount of fibrosis around individual large vessels; 2) no epithelium in the sample; 3) Modest amount of liver tissue; 4) cornea, iris and lens not present; 5) few small areas with infiltration; 6) a smaller focus, possibly pressure influence from isolation; 7) less infiltration towards the lumen.

nature portfolio

Corresponding author(s): Jakob B. Hansen
Zachary Gerhart-Hines

Last updated by author(s): Jul 23, 2024

Reporting Summary

Nature Portfolio wishes to improve the reproducibility of the work that we publish. This form provides structure for consistency and transparency in reporting. For further information on Nature Portfolio policies, see our Editorial Policies and the Editorial Policy Checklist.

Statistics

For all statistical analyses, confirm that the following items are present in the figure legend, table legend, main text, or Methods section.

n/a	Confirmed	
☐	☒	The exact sample size (*n*) for each experimental group/condition, given as a discrete number and unit of measurement
☐	☒	A statement on whether measurements were taken from distinct samples or whether the same sample was measured repeatedly
☐	☒	The statistical test(s) used AND whether they are one- or two-sided *Only common tests should be described solely by name; describe more complex techniques in the Methods section.*
☒	☐	A description of all covariates tested
☐	☒	A description of any assumptions or corrections, such as tests of normality and adjustment for multiple comparisons
☐	☒	A full description of the statistical parameters including central tendency (e.g. means) or other basic estimates (e.g. regression coefficient) AND variation (e.g. standard deviation) or associated estimates of uncertainty (e.g. confidence intervals)
☐	☒	For null hypothesis testing, the test statistic (e.g. *F*, *t*, *r*) with confidence intervals, effect sizes, degrees of freedom and *P* value noted *Give P values as exact values whenever suitable.*
☒	☐	For Bayesian analysis, information on the choice of priors and Markov chain Monte Carlo settings
☒	☐	For hierarchical and complex designs, identification of the appropriate level for tests and full reporting of outcomes
☒	☐	Estimates of effect sizes (e.g. Cohen's *d*, Pearson's *r*), indicating how they were calculated

Our web collection on statistics for biologists contains articles on many of the points above.

Software and code

Policy information about availability of computer code

Data collection
Oxygen consumption, carbon dioxide production and food intake were recorded using the Promethion core system (Sable Systems International) with data processing using OneClickMacroV2.52.1 and Macrointerpretersetup_v2_47 or the Phenomaster Home Cage System (TSE Systems) with PhenoMaster software v.8.2.9. Continuous body temperature and motor activity were measured with G2 E-Mitter telemetric devices (Starr Life Sciences) or with RFID temperature transponders (UCT-2112 microchips, Unified Information Devices). E-mitter data was recorded by placing ER4000 Receivers under the cages within the TSE cabinet. Temperature data was integrated in the Phenomaster software. RFID temperature transponder data was recorded by using UID Mouse Matrix system (Unified Information Devices) in combination with the Sable system.

Data analysis
Statistical analyses were performed using GraphPad Prism v.9.5.1 or SPSS v.29.0.2.0 (IBM). The source code used to analyze the snRNA-seq and produce figures is available at https://github.com/perslab/Sass-2024/. All analyses were performed in Rstudio (2022.07.2+576) with R (4.1.3). Data were loaded and manipulated using data.table (1.14.2) and tidyverse (1.3.1). Linkage disequilibrium (LD) operations were performed using plink1.975, ggLD (https://github.com/mmkim1210/ggLD), and LDLink77. All results can be reproduced by following the code available. in: https://github.com/MarioGuCBMR/nk2r_hk1_genetics. Specific statistical tests were described in relevant figures, figure legends, or supplemental material.

For manuscripts utilizing custom algorithms or software that are central to the research but not yet described in published literature, software must be made available to editors and reviewers. We strongly encourage code deposition in a community repository (e.g. GitHub). See the Nature Portfolio guidelines for submitting code & software for further information.

Data

> We have included the following Data Availability statement in the methods section of the manuscript:
> snRNA-seq data are deposited to the NCBI Gene Expression Omnibus under accession number: GSE276735. Source data for all studies presented are provided with this paper.
>
> I can confirm that there are no data generated and included in this paper that are restricted.
>
> We have also included analysis of previously published human genetic cohorts:
> 1. https://www.sdu.dk/da/sif/rapporter/2011/inuit_health_in_transition
> 2. https://www.sdu.dk/da/sif/rapporter/2019/befolkningsundersoegelsen_i_groenland
> 3. Bjerregaard, P. et al. Inuit health in Greenland: a population survey of life style and disease in Greenland and among Inuit living in Denmark. Int. J. Circumpolar Health 62 Suppl 1, 3–79 (2003).
> 4. T2D Knowledge Portal (http://t2d.hugeamp.org) was used for analyzing HbA1c associations.
> 5. Open Target Genetics (OTG) were utilized to query the variant-to-gene (V2G) scores used for gene prioritization and the associations of causal variants with expression quantitative trait loci (eQTLs).

Research involving human participants, their data, or biological material

Reporting on sex and gender	n/a
Reporting on race, ethnicity, or other socially relevant groupings	n/a
Population characteristics	n/a
Recruitment	n/a
Ethics oversight	n/a

Note that full information on the approval of the study protocol must also be provided in the manuscript.

Field-specific reporting

Please select the one below that is the best fit for your research. If you are not sure, read the appropriate sections before making your selection.

☒ Life sciences   ☐ Behavioural & social sciences   ☐ Ecological, evolutionary & environmental sciences

For a reference copy of the document with all sections, see nature.com/documents/nr-reporting-summary-flat.pdf

Life sciences study design

All studies must disclose on these points even when the disclosure is negative.

Sample size	No statistical methods were applied to predetermine sample size for in vivo pharmacology experiments. Sample sizes were determined based on previous experience with related experimental setups (PMID: 34048700).
Data exclusions	For continuous body temperature measurements in mice, four E-mitters malfunctioned after implantation and measurements of these mice were excluded from analysis. During the s.c. vs ICV crossover study, two mice had to be sacrificed due to health concerns related to the surgeries. In the NHP study, some measurements for the blood parameters failed and couldn't be repeated due to limited or no remaining sample.
Replication	To ensure reproducibility and replication of our core findings, animals studies were independently and successfully repeated by four researchers (FS, JPE, JBH, TM) independently as well as a third party, contract research organization (Gubra) and comparable effect sizes were observed/confirmed.
Randomization	Mice were grouped based on body weight, such that each group had the same average body weight upon study start. Randomization for

Randomization	nonhuman primates was not applicable as all animals received increasing doses of compound and then a monitored period of drug washout.
Blinding	The mouse studies were not blinded to the investigators but were conducted according to standardized protocols and procedures. The NHP study was not blinded to investigators as all animals received dose escalation and wash-out of the NK2R agonist compound. This is common practice for safety and dose-finding studies.

Reporting for specific materials, systems and methods

We require information from authors about some types of materials, experimental systems and methods used in many studies. Here, indicate whether each material, system or method listed is relevant to your study. If you are not sure if a list item applies to your research, read the appropriate section before selecting a response.

Materials & experimental systems

n/a	Involved in the study
☐	☒ Antibodies
☐	☒ Eukaryotic cell lines
☒	☐ Palaeontology and archaeology
☐	☒ Animals and other organisms
☒	☐ Clinical data
☒	☐ Dual use research of concern
☒	☐ Plants

Methods

n/a	Involved in the study
☒	☐ ChIP-seq
☒	☐ Flow cytometry
☒	☐ MRI-based neuroimaging

Antibodies

Antibodies used	FOS (Cell Signalling, 2250), GFP (Aves Laboratories, 1020), AKT (Cell Signaling, 9272), pAKT T308 (Cell Signalling, 9275), Tyrosine hydroxylase (Abcam, ab137869), UCP1 (Abcam, ab10983), Alexa Fluor 488 and 568 secondary antibody (Invitrogen, A-11039, A-11011), Anti-rabbit IgG secondary (Jackson Immuno Research, 111-035-144, 1:5000)
Validation	All antibodies have been validated for use in western blotting in mice. Validation statements from the websites of the antibody companies include: FOS - This antibody detects endogenous levels of total c-Fos protein. The antibody does not cross-react with other Fos proteins, including FosB, FRA1 and FRA2. c-Fos (9F6) Rabbit mAb #2250 non-specifically stains fixed frozen mouse spleen and liver by immunofluorescence (Nakabeppu, Y. and Nathans, D. (1991) Cell 64, 751-9.) GFP - This antibody was validated by western blot analysis (1:5000 dilution) and immunohistochemistry (1:500 dilution) using transgenic mice expressing the GFP gene product. AKT - The Akt Antibody detects endogenous levels of total Akt1, Akt2 and Akt3 proteins. The antibody does not cross-react with related kinases (e.g. Cross, D.A. et al. (1995) Nature 378, 785-9.) pAKT T308 - Phospho-Akt (Thr308) Antibody detects endogenous levels of Akt only when phosphorylated at Thr308 (e.g. Cross, D.A. et al. (1995) Nature 378, 785-9.) Tyrosine hydroxylase - Monoclonal antibody made using Abcam hybridoma-based technology and validated at 1/500 concentrations for western blotting (PMID: 37179330) UCP1 - Synthetic Peptide within Human UCP1 aa 100-200 conjugated to Keyhole Limpet Haemocyanin (PMID: 35675775) For Secondary antibodies: For FOS (Cell Signalling, 2250, 1:1000) and GFP (Aves Laboratories, 1020, 1:1000), we used a secondary antibody conjugated to Alexa Fluor 488 and 568 (Invitrogen, A-11039 (anti-chicken IgG), A-11011 (anti-rabbit IgG), 1:250) For AKT (Cell Signaling, 9272, 1:1000), pAKT T308 (Cell Signalling, 9275, 1:1000), Tyrosine hydroxylase (Abcam, ab137869, 1:1000), UCP1 (Abcam, ab10983, 1:7500), we used peroxidase-conjugated AffiniPure™ Goat Anti-Rabbit IgG (H+L) (Jackson Immuno Research, 111-035-144, 1:5000)

Eukaryotic cell lines

Policy information about cell lines and Sex and Gender in Research

Cell line source(s)	COS-7 cells were purchased from ATCC.
Authentication	Cell lines were not authenticated
Mycoplasma contamination	Cell line was routinely tested for mycoplasma contamination and found to be negative for mycoplasma contamination.

Commonly misidentified lines (See ICLAC register)	No commonly misidentified cell lines were used.

Animals and other research organisms

Policy information about studies involving animals; ARRIVE guidelines recommended for reporting animal research, and Sex and Gender in Research

Laboratory animals	C57Bl/6NRj (WT) mice, B6.V-Lepob/JRj (ob/ob) mice and RjOrl:SWISS (CD-1®) mice were purchased from Janvier Labs (Le Genest-Saint-Isle, France). B6.129S4-Mc4rtm1Lowl/J (Mc4r KO), Ccktm1.1(cre)Zjh/J, B6.129-Leprtm3(cre)Mgmj/J, Calcrtm1.1(cre)Mgmj/J, B6;129-Gt(ROSA)26Sortm5(CAG-Sun1/sfGFP)Nat/J and Gt(ROSA)26Sortm1(CAG-EGFP/Rpl10)Dolsn mice were purchased from the Jackson Laboratory (Maine, US). The Ucp1 KO line was kindly provided by Prof. Karsten Kristiansen (University of Copenhagen). Nk2r conditional KO mice and B6N-Tacr2tm1Zpg (Nk2r floxed) mice, were generated by GenOway (Lyon, FR). These mice were also used in the studies where AAV-Cre and AAV-GFP viruses were injected into the DVC to generate NK2R-DVC-Cre and NK2R-DVC-GFP mice, respectively. Adult male and female mice aged 12-30 weeks were used for all studies. For the nonhuman primate study, the mean ages of the rhesus macaques at study start were 20.6 years old (standard deviation=2.1) for females and 15.4 years old (standard deviation=4.3) for males.
Wild animals	Study did not involve wild animals.
Reporting on sex	Murine findings are reported for male and female mice as indicated in results, figures, figure legends and methods. NHP data are reported for both male and female macaques. Human genetic analysis includes both males and females.
Field-collected samples	Study did not involve samples collected from the field.
Ethics oversight	All mouse studies were approved by The Danish Animal Experiments Inspectorate (permit number: 2018-15-0201-01441 and 2023-15-0201-01386) and the University of Copenhagen (project number: P20-015, P22-209). Animal experiments performed at the University of Michigan were approved by the University of Michigan Committee on the Use and Care of Animals (Protocol#00011066) and in accordance with Association for the Assessment and Approval of Laboratory Animal Care and National Institutes of Health guidelines. The nonhuman primate studies were conducted in compliance with all federal regulations, including the United States Animal Welfare Act. Studies were reviewed and approved by the OHSU/ONPRC Institutional Animal Care and Use Committee. The ONPRC is accredited by AAALAC International.

Note that full information on the approval of the study protocol must also be provided in the manuscript.